REPORT DOCUMENTATION PAGE

Form Approved
OMB No. 0704-0188

1. AGENCY USE ONLY *(Leave blank)*	2. REPORT DATE	3. REPORT TYPE AND DATES COVERED
	1/31/95	Final 8/1/94 - 1/31/95

4. TITLE AND SUBTITLE

Fourier Synthesis Lithographic Machine for Large Panel Display Fabrication

5. FUNDING NUMBERS

DAAH04-94-C-0029

6. AUTHOR(S)

Lev Sadovnik

7. PERFORMING ORGANIZATION NAME(S) AND ADDRESS(ES)

Physical Optics Corporation
20600 Gramercy Place, Building 100
Torrance, California 90501

8. PERFORMING ORGANIZATION REPORT NUMBER

3283

9. SPONSORING / MONITORING AGENCY NAME(S) AND ADDRESS(ES)

Attn: Richard O. Ulsh
US Army Research Office
P.O. Box 12211
Research Triangle Park, NC 27709-2211

10. SPONSORING / MONITORING AGENCY REPORT NUMBER

ARO 33577.1-EL-SBI

11. SUPPLEMENTARY NOTES

12a. DISTRIBUTION / AVAILABILITY STATEMENT

Unlimited

12b. DISTRIBUTION CODE

13. ABSTRACT *(Maximum 200 words)*

This report addresses the development of a substitute for conventional lithographic technologies used to fabricate flat panel displays. Conventional technology has several weaknesses: an image field ≤ 50 mm × 50 mm, a need for expensive projection equipment and precision stepper machines with a positioning accuracy of ~0.25 μm and depth of focus of ~1 μm; and the necessity to use complicated mask technologies which pollute the environment. Physical Optics Corporation (POC) is developing a new Fourier synthesis lithography technology which will provide a field size of ~500 mm × 500 mm without optical distortion or aberration. During Phase I, POC completed an optimization procedure to find the exact harmonic exposure to create the highest edge gradient in a synthetic lithographic pattern. We produced a comprehensive computer model of photoresist multiple exposure, and confirmed it experimentally. We also experimentally confirmed our simulation of the lateral propagation of the development process in photoresist. We completely designed the proposed Fourier synthesis lithographic machine (FSLM). We anticipate that development of this new technology will lead to the construction of a full scale FSLM.

"Original contains color plates: All DTIC reproductions will be in black and white"

14. SUBJECT TERMS

Flat Panel Display, Lithographic Technology, Harmonics, Interference, Photoresist

15. NUMBER OF PAGES

52

16. PRICE CODE

17. SECURITY CLASSIFICATION OF REPORT	18. SECURITY CLASSIFICATION OF THIS PAGE	19. SECURITY CLASSIFICATION OF ABSTRACT	20. LIMITATION OF ABSTRACT
Unclassified	Unclassified	Unclassified	SAR

DISCLAIMER NOTICE

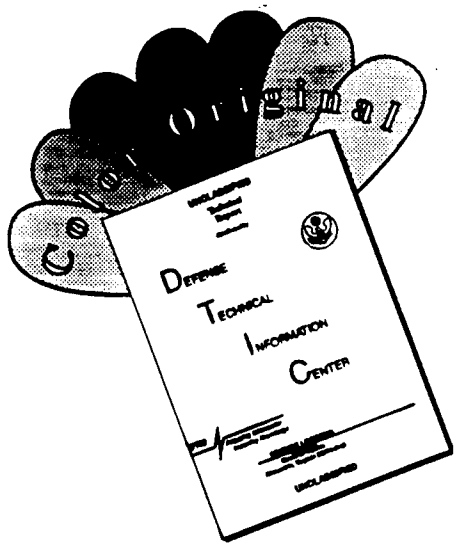

THIS DOCUMENT IS BEST QUALITY AVAILABLE. THE COPY FURNISHED TO DTIC CONTAINED A SIGNIFICANT NUMBER OF COLOR PAGES WHICH DO NOT REPRODUCE LEGIBLY ON BLACK AND WHITE MICROFICHE.

1.0 INTRODUCTION

Recently, flat panel display (FPD) devices such as liquid crystal displays (LCDs), plasma displays, vacuum fluorescent displays (VFDs), and electro-luminescent displays (ELDs) have garnered considerable attention because of their desirable characteristics: thin profile, light weight, low-voltage operation, and low power consumption. None of these features characterize currently available CRTs. ***The growing demand for large FPD devices in both military and civilian markets was the basis for this project.***

Of all FPD technologies, this country's competitive position is worst in the LCDs. Most passive matrix (PMLCD) and active matrix (AMLCD) liquid crystal displays are made offshore, predominantly in Japan. Inadequate manufacturing tooling is partially to blame for the absence of real progress in this area.

The proliferation of FPD devices and systems requires an efficient lithographic process for FPD screen fabrication, especially for large-area FPDs. Conventional stepper machines cascade the exposure procedures to cover the whole panel area. The fastest stepper machine to date for the production of FPD screens is the MRS 4500R, which yields a maximum square image of 56.5 mm × 56.5 mm per step.

Physical Optics Corporation (POC) is developing ***a system to replace traditional projection optics*** which use stencils and complicated objectives as well as precision positioning devices. ***POC's system creates a holographic exposure field built up from a limited number of harmonics.*** The hardware incorporates reflective optics and devices which use collimated beams with precisely controlled direction. For various ranges of dimensions, different versions of the device are being investigated.

Whereas a conventional stepper machine can produce a 500 mm × 500 mm FPD in 100 steps, the technology being developed here can produce an FPD of that same size using a limited number of harmonics (~18), with all harmonics affecting all areas of the display, more than five times as fast.

2.0 PROJECT TASKS

The total effort under this project was organized into five tasks, listed below. Sections 3 through 15 describe in detail the work performed and the results of that work. Section 16 presents the conclusions and lays out the direction in which the Phase II effort should proceed.

Task 1. Calculate the individual Fourier components' amplitudes. The crucial issue of the proposed approach is how accurately can a lithographic pattern be synthesized using a limited number of harmonics.

Task 2. Develop and experimentally evaluate mathematical and programming techniques for simulating the processes of photoresist exposure and development.

Task 3. Analyze the structural details of different types of hardware in several ranges of dimensions with respect to the demands of the theory of image formation.

Task 4. Confirm the theoretical conclusions through experimental results.

3.0 CREATING ONE-DIMENSIONAL STRUCTURES WHICH ARE INSENSITIVE TO VARIATIONS IN EXPOSURE

A significant difficulty confronting this approach is that an object created with a reasonably small number of harmonics tends to be irregular in shape in a way that leaves limited tolerance for the variability of the exposure and developing processes. The goal of this project is to develop a system which will enhance this tolerance while still using only a small number of harmonics.

POC conducted computer simulations of the optical synthesis of 1-D rectangular profiles which are insensitive to variations in exposure. The width a_x of the rectangular profile was set at 1.2 μm. The profile s(x) is shown in Figure 1.

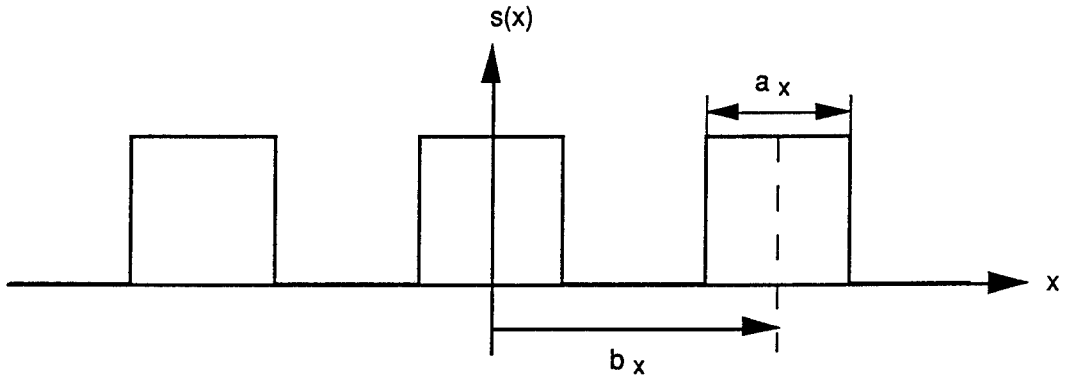

Figure 1
One-dimensional rectangular profile to be synthesized.

For simplicity, we assume $b_x = 2a_x$. The Fourier transform of s(x) is shown in Figure 2; s(x) can be approximated as the sum of a limited number of harmonics as in Eq. (1).

$$s(x)=\sum_{k=0}^{N}\frac{\sin(\pi a_k k/b_x)}{\pi k/b_x}2\cos\{(2\pi k/b_x)x\} \quad , \tag{1}$$

where N is the total number of harmonics used for synthesis. The setup used for the modeling (see Figure 3) enables us to record cosinusoidal harmonics

$$G(x)=G_o\left[1+\cos\left(\frac{2\pi}{\lambda}2x\sin\theta\right)\right] \quad , \tag{2}$$

where G(x) is the photoresist exposure and G_o is the exposure bias.

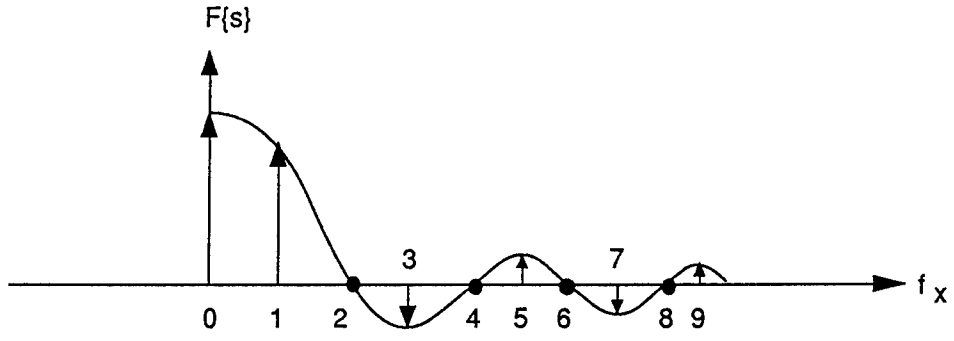

Figure 2
Fourier transform of the function shown in Figure 1.

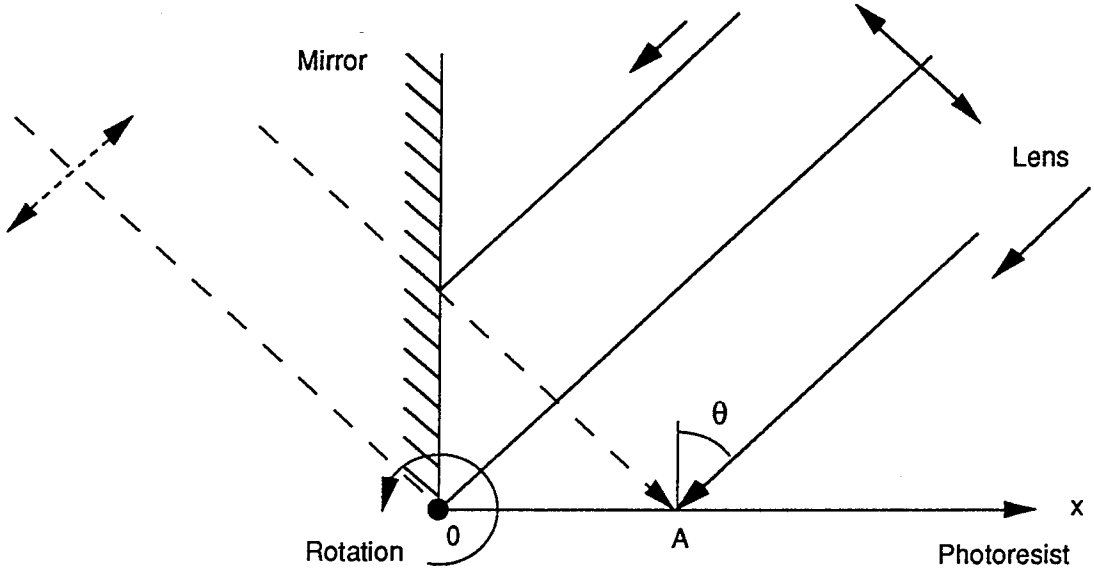

Figure 3
Fourier synthesis recording setup.

It follows from Eq. (2) that:

1. Since our setup cannot produce variable sign harmonics as required by Eq. (1), all harmonics must include a bias and remain positive.

2. This setup does not produce harmonics with phase shifts. The point at which the phase is zero is x = 0 in Figure 3. In order to introduce a phase shift, as for

harmonics number 3 and 7 for instance, we need to shift the photoresist plate by half of the corresponding period.

As a result, the setup in Figure 3 is capable of generating the following set of harmonics:

$$s(x)=\sum_{k=1}^{N}\left\{\left|\frac{\sin(\pi a_x k/b_x)}{\pi k/b_x}\right|+\frac{\sin(\pi a_x k/b_x)}{\pi a_x k/b_x}\cos\{(2\pi k/b_x)x\}\right\} . \qquad (3)$$

In order to demonstrate the feasibility of our approach, we decided to synthesize a one dimensional rectangular profile with a_x = 1.2 μm, b_x = 2.4 μm, and illumination at a wavelength of λ = 0.414 μm. It follows from Eqs. (2) and (3) that

$$\frac{k}{b_x}=\frac{2\sin\theta_k}{\lambda}; \quad \text{or} \quad \sin\theta_k=\frac{k\lambda}{2b_x} . \qquad (4)$$

To form the rectangular profile, we use harmonics numbers 1, 3, 5, 7, and 9 (see Figure 2). The recording angles θ_k and their respective required shifts are shown in Table 1.

Table 1 Recording Angle and Lateral Shift Required to Record Harmonics

Harmonic Number	θ_k (deg)	Shift (μm)
1	4.93	0
3	15.01	0.4
5	25.53	0
7	37.15	0.17
9	50.89	0

These harmonics produce the accumulated intensity distribution shown in Figure 4.

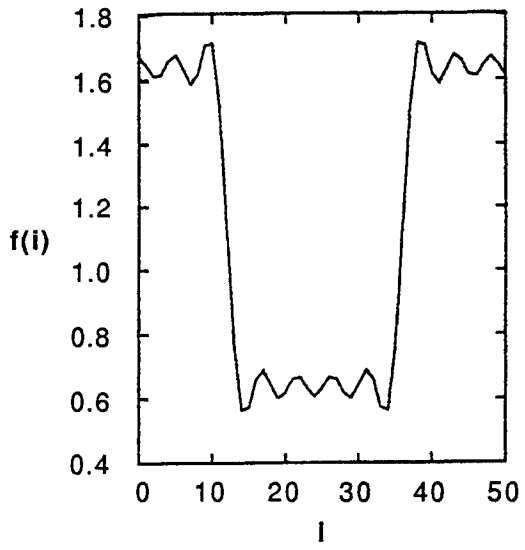

Figure 4
Accumulated intensity distribution resulting from harmonic synthesis.

The relative intensity is f(i). Step i used in the calculations is 0.05 μm. To produce an ideal rectangular profile one would like to set the exposure half way between the top and the bottom of the exposure curve, so that at the level of intensity f(i) = 1.13 (see Figure 4) the photoresist would be removed completely. The tolerance to the deviation in the intensity which produces a structure without strips in the transparent portion of the image and without a transparent fringe in the opaque portion is ±0.45 or D = ±39% of the cutoff level. A deviation of about 10% from the nominal cutoff level of the intensity results in a deviation in the width of the rectangular form, U = 0.03 μm. Thus,

$$\begin{cases} D = \pm 39\% \\ U = 0.03\mu m \end{cases} . \qquad (5)$$

Displacements of 0.4 and 0.17 μm presented in Table 1 are difficult to realize with the required precision of about 0.03 μm. We investigated the possibility of forming the rectangular profile without using these negative harmonics. To do that, we add the absolute value of the amplitude of the third harmonic to all of the harmonics in the sum. The result is shown in Figure 5.

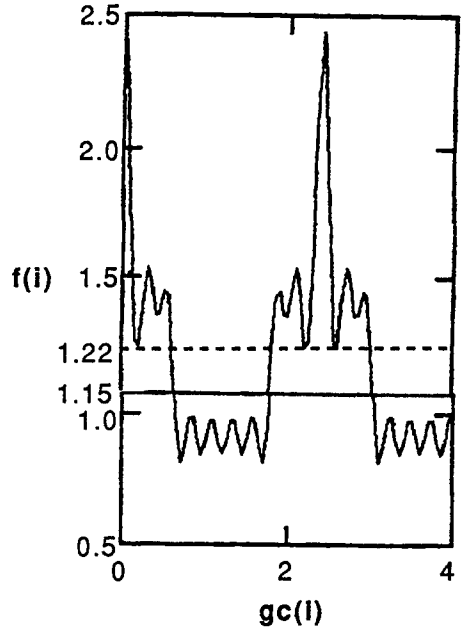

Figure 5
Simulation of a rectangular profile without negative harmonics.

In Figure 5, the actual dimension of gc(i) is in microns. We used nine nonzero harmonics, since harmonics number 2, 4, 6, and 8 are now nonzero. From Figure 5, the level of intensity at which the photoresist material will be removed completely is set to about 1.22, and

$$\begin{cases} D = \pm 9.5\% \\ U = 0.05\mu m \end{cases} . \tag{6}$$

The actual depth response of the photoresist measured previously is shown in Figure 6, where vbm is the depth (μm) of the remaining photoresist and bm is the exposure in mJ/cm^2. We set the level of completely removed photoresist at 1.15 as for Figure 5. In this case we chose the maximum exposure at the point gc = 0 (see Figure 5) to be

$$E_{max} = \frac{2.48}{1.15} \cdot 1200 = 2500 \text{ mJ/cm}^2 , \tag{7}$$

where 1200 mJ/cm^2 is the exposure at which the material is completely removed (see Figure 6). The relative amplitudes of the harmonics in this case are shown in Table 2. The results of computer simulation are shown in Figure 7.

Table 2 Amplitude of Harmonics Used for Rectangular Profile Synthesis

N	1	2	3	4	5	6	7	8	9
Amplitude	1	0.25	0	0.25	0.4	0.25	0.143	0.25	0.33

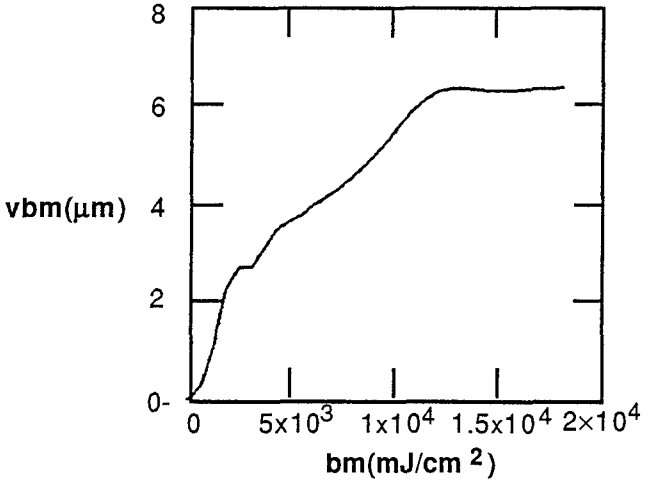

Figure 6
Depth response curve of the photoresist. Here, vbm is the depth of the remaining photoresist and bm is the exposure in mJ/cm^2.

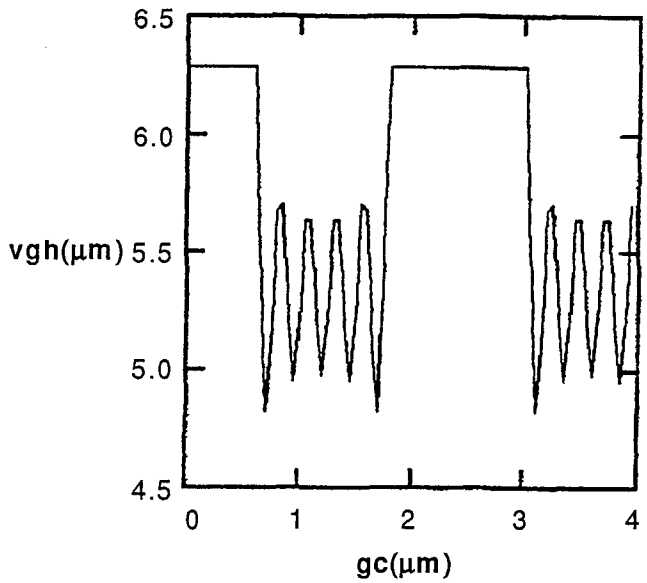

Figure 7
Rectangular profile formed on photoresist using only positive harmonics.

The depth vgh = 6.3 μm reflects complete removal of photoresist. The results presented in Figures 5 and 7 demonstrate considerable degradation of the characteristics D and U (Eq. (5)). It is possible to improve these characteristics, however, if we add to each of the other harmonics a constant with the amplitude of the seventh harmonic, and if the amplitude of the third harmonic is set to zero. This significantly improves the dynamic characteristics:

$$\begin{cases} D = \pm 27\% \\ U = 0.037\,\mu m\,. \end{cases} \qquad (6)$$

The resulting image is shown in Figure 8. The computer simulated photoresist profile is shown in Figure 9.

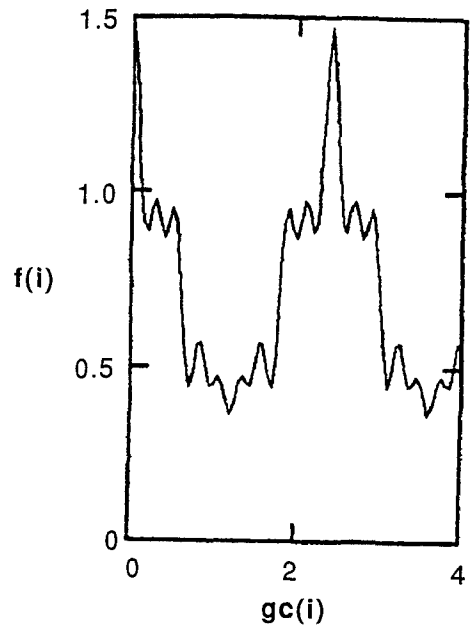

Figure 8
Intensity simulation of the improved rectangular form.

The fringes in the dark (undeveloped) regions will not affect the pattern, since a photoresist depth of at least 1 μm is preserved.

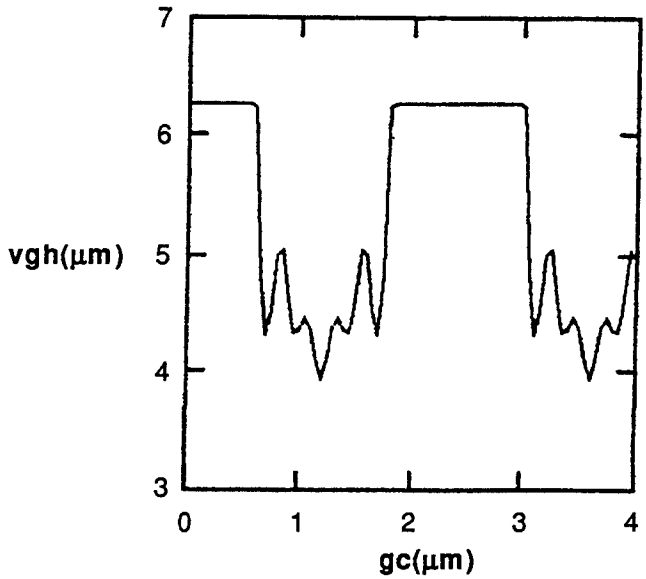

Figure 9
Form of the rectangular profile on photoresist.

4.0 HOW TO SYNTHESIZE A PERIODIC RECTANGULAR PROFILE WITHOUT SHIFTING THE MIRROR

The preceding section explained that to avoid the expensive and complicated necessity of shifting the mirror a fraction of a micron to build up negative harmonics (see also Section 8) it is possible to use the noise spectrum of the object (the theoretical rectangular image) to synthesize the amplitude of the seventh harmonic. This process is in need of clarification.

Section 3 examined the case of synthesizing a periodic rectangular profile with a period $b_x = 2.4$ μm and a rectangular profile line width of $a_x = 1.2$ μm. The summation of all harmonics was normalized by the period b_x. We discovered that the best way to eliminate the need for negative harmonics is to bias the Fourier spectrum by a constant Δ. As a result, the new intensity distribution function becomes

$$F(x) = \Delta \sin\left[\pi(2K+1)x/b_x\right] / \left[b_x \sin(\pi x/b_x)\right] \quad , \qquad (7)$$

where K is the number of harmonics utilized in the positive frequency domain. When $b_x = 2.4$ μm, $a_x = 1.2$ μm, and $\Delta = 1$, the function F(x) is as shown in Figure 10.

Figure 11 shows the image of a rectangular object with its Fourier spectrum biased by the amplitude of the third harmonic. The diagonally hatched zone is the region within which it is possible to vary the exposure L while still completely removing the photoresist. The purpose of this research is to maximize this region in relation to the total amplitude of exposure.

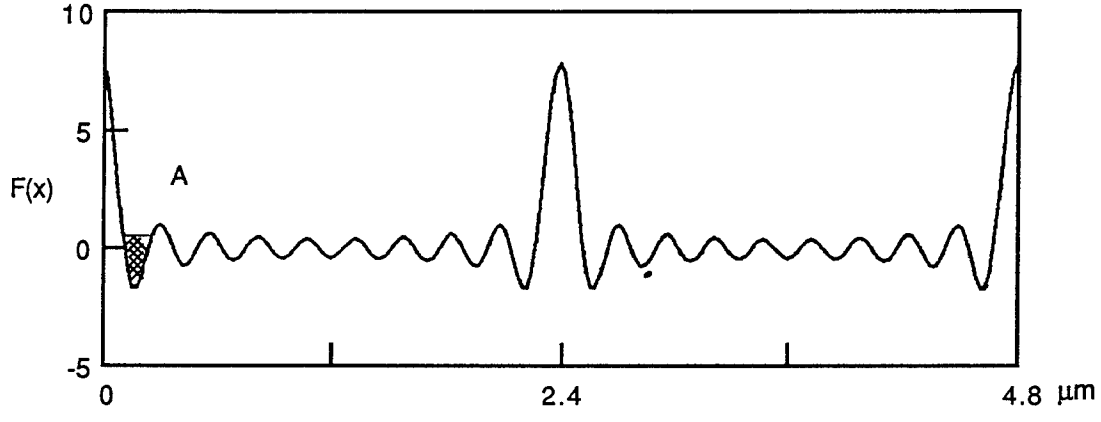

Figure 10
The function F(x) which is added to our object.

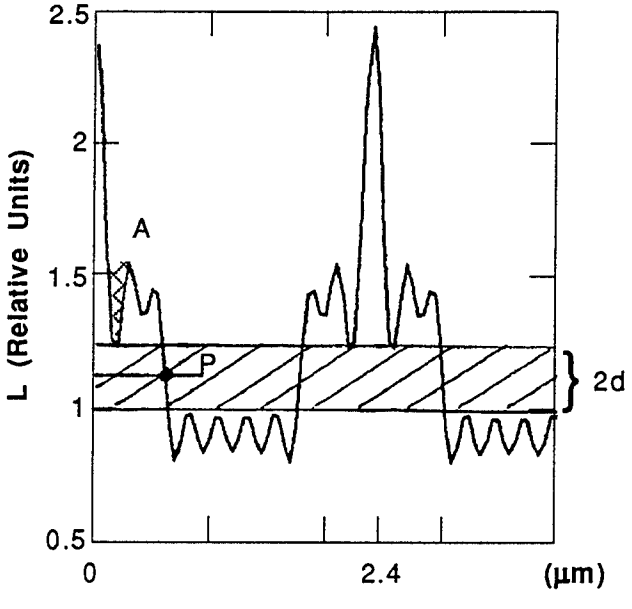

Figure 11
Synthesis of a rectangular profile without the use of negative harmonics.

Essential to the determination of the exposure tolerance area is the depth of the crosshatched area A in Figures 10 and 11. Reducing the amplitude of the bias function Δ in Eq. (7) increases the range over which the exposure completely removes the material of the photoresist -- 2d (see Figure 11). We can also achieve the same effect by distorting the ratio between the amplitude of the third harmonic, and of some other harmonic. Let us investigate the results of this operation. Figure 12(a) shows the rectangular object created using nine undistorted harmonics. Figure 12(b) shows its first derivative.

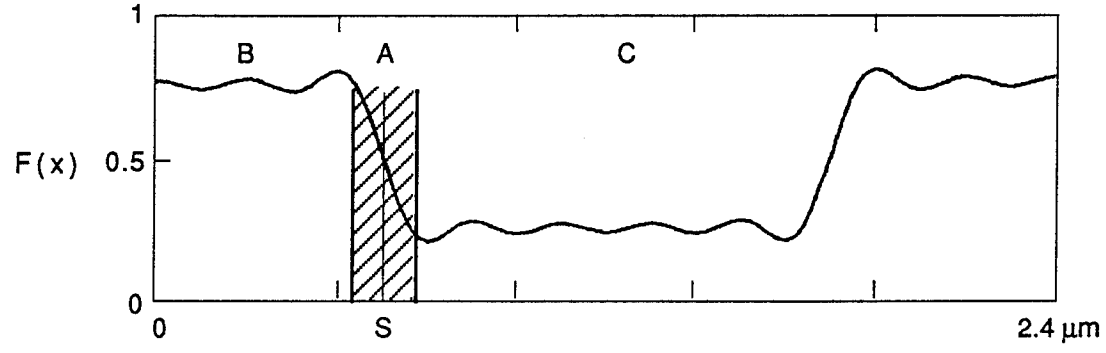

Figure 12(a)
Rectangular object created using nine undistorted harmonics.

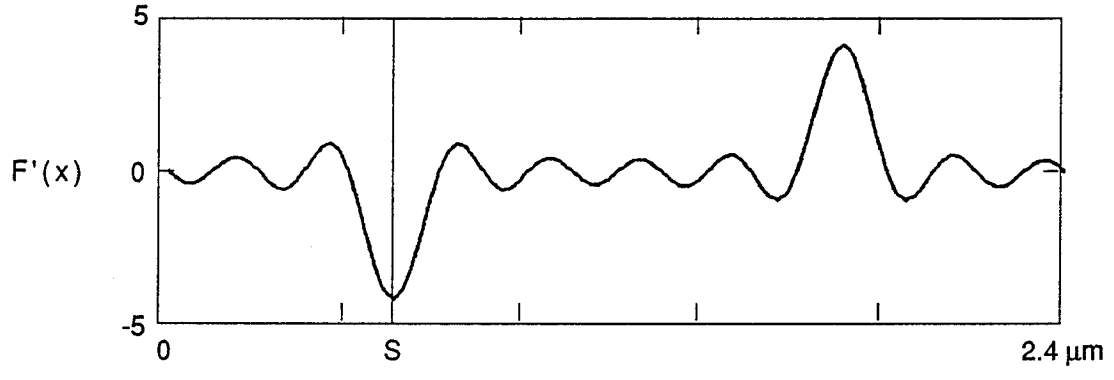

Figure 12(b)
First derivative of rectangular object.

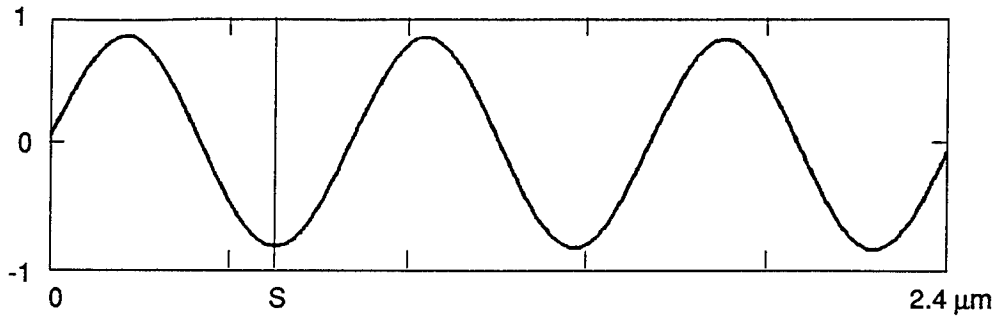

Figure 12(c)
First derivative of third harmonic.

Figure 12(c) shows the first derivative of the third harmonic. At point S in Figures 12(a), (b), and (c), the derivative of the object is at its absolute value maximum, and as a result an error in the level of exposure produces the minimum deviation in the width of the rectangular object. As can be observed in Figure 12(c), the reduction in amplitude of the third harmonic to the level of the seventh harmonic does not distort the shape of the edge structure in the crosshatched zone in Figure 12(a). The changes in zones B and C are smoothed out in the process of developing the photoresist.

Let us now consider the behavior of the dynamic characteristics D and V. D is the relative range of cut-off levels, and V is the variation in width of the rectangular object as a result of varying the cut-off level L about 0.1.

$$D = d/L,\ V_0 \approx (-2/F') \times (L/10), \tag{8}$$

where F' is a derivative of the object at point P (see Figure 11). In order to reduce Δ, and thus to reduce the crosshatched area A in Figures 10 and 11, we reduce the amplitude of the third harmonic. In this process, d increases and L decreases. Hence, the stability of D is improved. If we reduce the amplitude of the third harmonic by a factor of Δ, L decreases by 9Δ because we are using nine harmonics. At the same time the derivative F', which we see in Figure 12(c) has an amplitude of 0.9, decreases by 0.9Δ. Hence,

$$U_1 \cong \left[2/(-5 + 0.9\Delta)\right]\left[(1.15 - 0.9\Delta)/10\right] \ . \tag{9}$$

In Figure 11, the function corresponding to b_x undergoes a shift in amplitude Δ = [sinc (3.5) - sinc (1.5)] $\times$ a_x/b_x = 0.06. Hence, υ_0 = 0.05 μm, and υ_1 = 0.03 μm are in good agreement with the data given in the Section 3. Further reducing Δ reduces the seventh harmonic and seriously distorts zone A (see Figure 12(a)).

5.0 SOME RESTRICTIONS ON THE FREQUENCY OF HARMONICS

The harmonic frequencies in our setup are subject to some restrictions. It follows from Section 3 that $f_K = K/b_x = 2\sin\theta_K/\lambda$, where θ_K is the incidence angle of the ray to the photoresist, and f_K = frequency. Since $\sin\theta_K$ cannot exceed 1, f_K cannot exceed $2/\lambda$. Less obvious are the restrictions in the area of low frequencies. Let us consider the scheme shown in Figure 13.

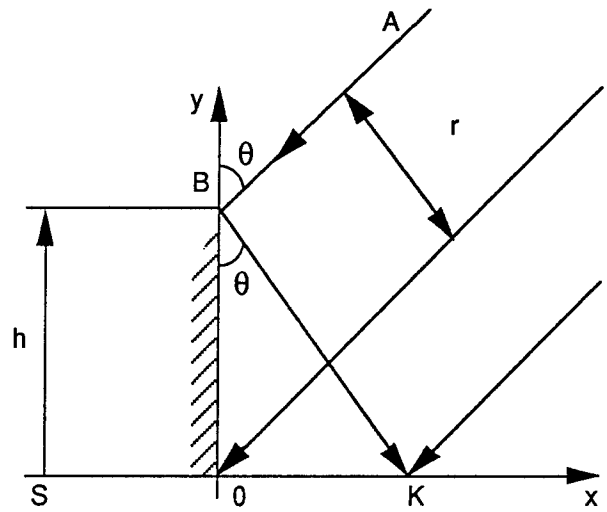

Figure 13
Synthesis setup.

As can be seen in Figure 13, as the frequency of the harmonic and the size of angle θ decrease there comes a moment when the edge ray A of the collimated bundle hits the edge of the mirror (at point B) which has altitude h, such that

$$\cos\theta = r/h. \qquad (10)$$

At this moment, the vignetting of the bundle begins. The form of the superposition zone is shown in Figure 14.

$$0\ K = h \tan \theta, \tag{11}$$

so we cannot reduce θ to zero. The minimum possible value of θ is $\tan(\theta_{min}) = 0\ K/h$, where $0\ K$ is the width of the interference domain. So the minimum value of f_K is $[2 \sin(\theta_{min})]\lambda$.

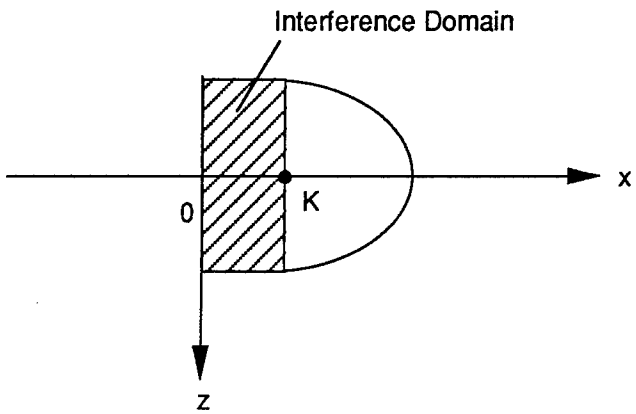

Figure 14
Form of the superposition domain.

6.0 ATTAINING LOWER FREQUENCY HARMONICS BY ROTATING THE RECORDING SETUP

Next we consider the possibility of reducing the frequencies of the harmonics by rotating the photoresist-mirror assembly. Let us investigate what will occur if we rotate the setup at an angle ϕ with respect to the y-axis (see Figure 15). The angle between the incident ray α and the y-axis is θ.

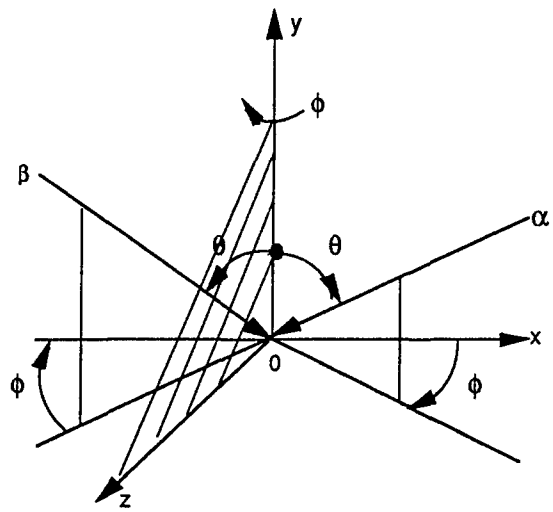

Figure 15
Setup rotated with respect to the y-axis.

If we take into account that our mirror lies in plane y0z, normal to the reflected beam, the ray β will have the direction shown in Table 3.

Table 3 Directions of Incident and Reflected Rays

	x	y	z
α	sin θ cos ϕ	cos θ	sin θ cos ϕ
β	- sin θ cos ϕ	cos θ	sin θ cos ϕ

In this case, the spatial phase difference ψ(x,y) at an arbitrary point on plane x0z is the difference between the distances from the point to the plane wave fronts connecting point 0 with the normals to rays α and β (see Figure 15), because at point 0 the interfering fronts are in phase.

$$\psi(x,z) = (x \sin\theta \cos\phi + z \sin\theta \sin\phi) - (-x \sin\theta \cos\phi + z \sin\theta \sin\phi) = 2x \sin\theta \cos\phi \,. \quad (12)$$

It follows from Eq. (12) that ψ is independent of coordinate z. Eq.(12) says that rotation through an angle ϕ with respect to the y-axis allows us to lower the minimal frequency of the recorded harmonic in proportion to cos ϕ.

7.0 CREATING A TWO-DIMENSIONAL IMAGE

To create two-dimensional images, Ref. [1] suggested rotating the photoresist plate around an arbitrary point K (see Figure 16).

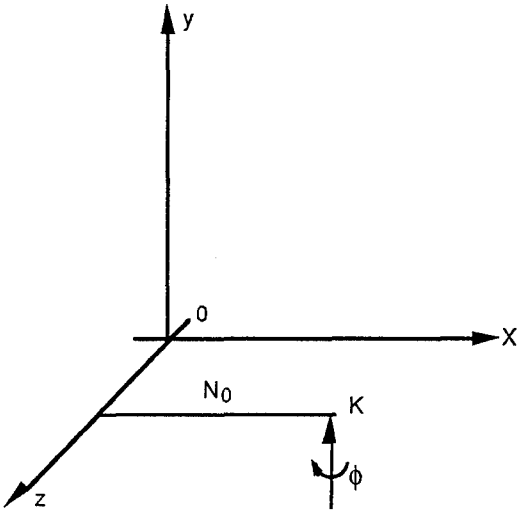

Figure 16
Rotating the photoresist plate.

However, it follows from Eq.(12) that zero phase difference for all harmonics is situated on line 0z, the intersection of the mirror and the photoresist plate. If we turn the photoresist plate around point K, the curve of zero phase is a circle with its center at point K (see Figure 17(a)).

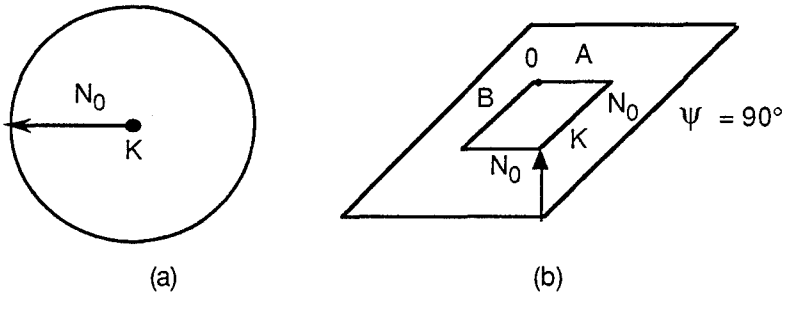

Figure 17
Locus of zero phase.

If the curve of zero phase is a circle with radius N_0, then at point K a harmonic with a given frequency will have phase $N_0/T(f)$, where T(f) is the period of a harmonic with frequency f. Therefore, we do not know where on the photoresist plate the phases of all harmonics in different directions are zero. Thus, this setup does not make it possible to obtain an image with arbitrary structure but rather is suitable only for producing a two-dimensional image with mutually perpendicular directions of harmonic generation. In this case, point 0, the crossing point of lines A and B of zero phase (see Figure 17(b)), is the origin point of the coordinate system. If we have harmonics in more than two different directions, it is necessary that the rotation axis lie in the plane of the mirror, in which case $N_0 = 0$.

8.0 INVESTIGATION OF HOW TO PRECISELY MOVE A MIRROR A FRACTION OF A MICRON

As an alternative, we have also investigated how best to shift the mirror a fraction of a micron to produce negative harmonics in the Fourier image of the rectangular object. For this purpose, it is possible to move the mirror very precisely using a piezoelectric translator with a capacitive sensor. Available piezoelectric translators can perform precision shifts under considerable working load. For example, Figure 18 shows the P-241 positioner (a product of Physik Instrumente), which can shift a mirror in the range of 5 μm with a precision of ≈0.02 μm under a load of 10,000 N. The construction of the mirror junction will depend on its required rate of movement. In the case of a very large mirror, it is necessary to take into consideration the stability of the mirror surface. Also, a translator with a capacitive sensor, such as those shown in Figure 18, costs about $10,000.

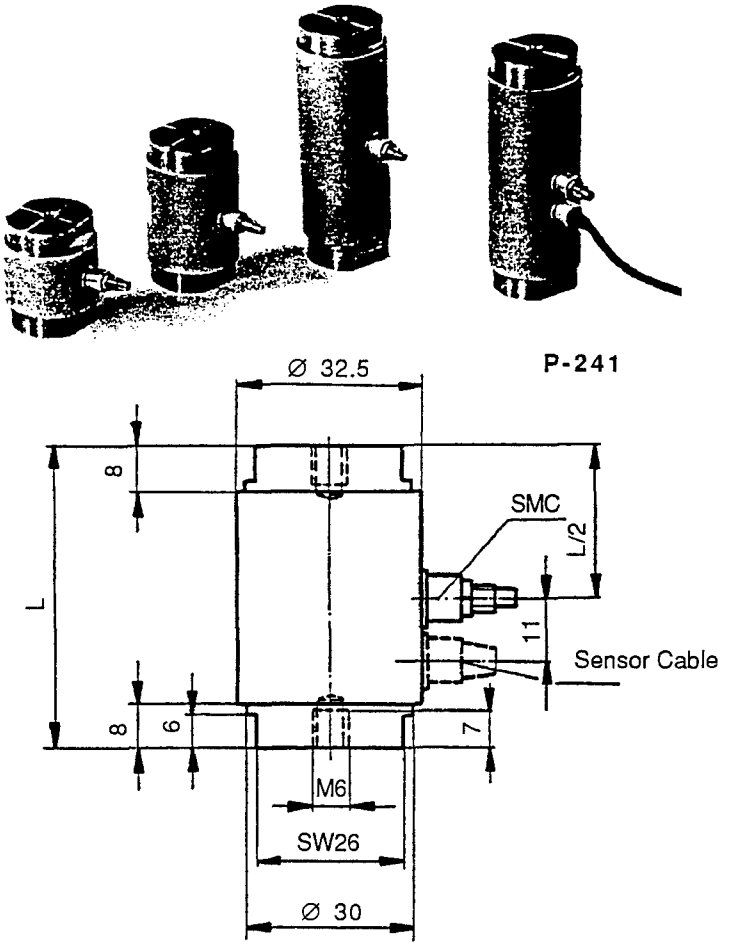

Figure 18
High load positioning elements Model P-241 with a load capacity up to 1000 kg (dimensions in mm).

9.0 INVESTIGATION OF HOW TO CREATE TWO-DIMENSIONAL OBJECTS ON A NEGATIVE PHOTORESIST

This section of the report considers how to create two-dimensional rectangular objects on negative photoresist. For this purpose we use only two series of harmonics propagating in mutually perpendicular directions. (The problems which appear when using more than two mutually perpendicular directions are discussed in Section 7.) As shown in Section 4, the image of one dimension of a rectangular object created without shifting the mirror has a positive hump in the center (see Figure 11). This is a considerable impediment to creating high-quality two-dimensional rectangular objects on positive photoresist, as can be illustrated using Figure 19.

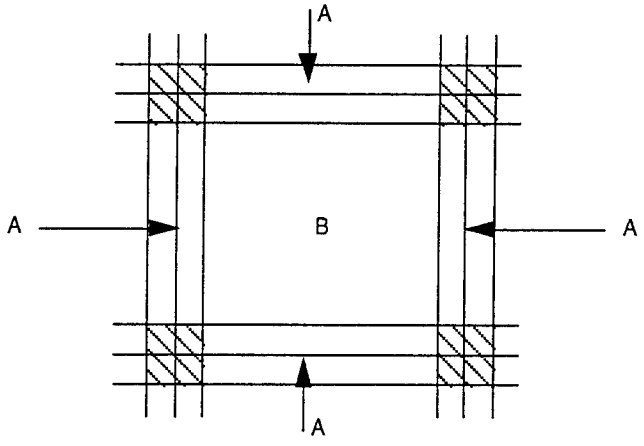

Figure 19
Ridges in the domain of minimum intensity.

As shown in Figure 19, the ridges (horizontal and vertical lines) in the center of the object inevitably cross the domains of minimum intensity A. Figure 19 suggests the idea of using domain B and negative photoresist to create a rectangular object of good shape. The depth curve of the negative photoresist is shown in Figure 20.

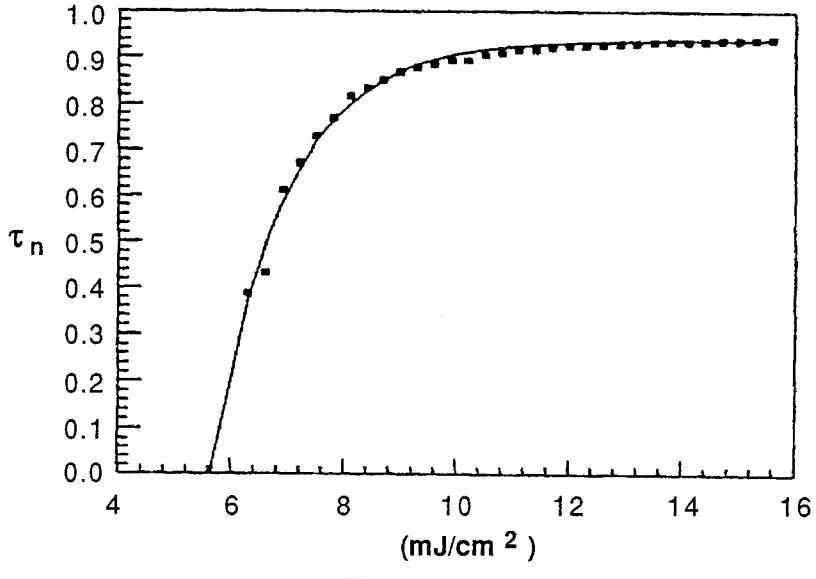

Figure 20
Depth curve of negative photoresist.

τ_n shows the thickness of negative photoresist remaining after developing. Eq. (13) represents the method of summating harmonics.

$$
\begin{aligned}
H(x,z) &= \sum_{K=1}^{N}\left[v(K) + v(K)\cos\left\{2p(K/b_x)x\right\}\right] \\
&+ \sum_{j=1}^{N}\left[w(j) + w(j)\cos\left\{2p(j/b_x)\right\}z\right] \\
v(K) &= P(K) + |P(M)|,\ w(j) = P(j) + |P(M)| \\
P(K) &= \sin(pa_xK/b_x)/(pK/b_x) \\
M &= 3 \text{ or } 7,\ a_x = 1{,}2 \text{ mm},\ b_x = 2,\ 4 \text{ m} \ ,
\end{aligned}
\tag{13}
$$

where N is the total number of harmonics. For the case of N = 1 (using only two mutually perpendicular harmonics), the result is shown in Figure 21.

The resulting shape is a square with rounded edges. The shape produced by using N = 3 and M = 3 is shown in Figure 22.

The results of using the seventh harmonic in the case of M = 3 are represented in Figure 23, which shows considerable improvement in the quality of edges and corners. However, Figure 23(c) shows that the dynamic range D of exposure is subject to some restrictions, because clear depressions have appeared. In this case, D = 28% of the whole depth of photoresist if we make the cutoff exposure coincide with 1.2 μm square edges.

The image which was obtained using the ninth harmonic demonstrates further improvement in form and reduction in D to D = 14%. Results are shown in Figure 24.

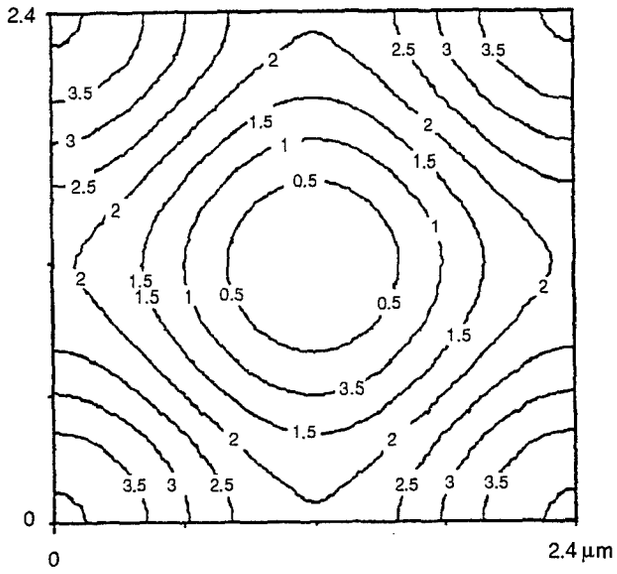

(a) 2-D Intensity Distribution

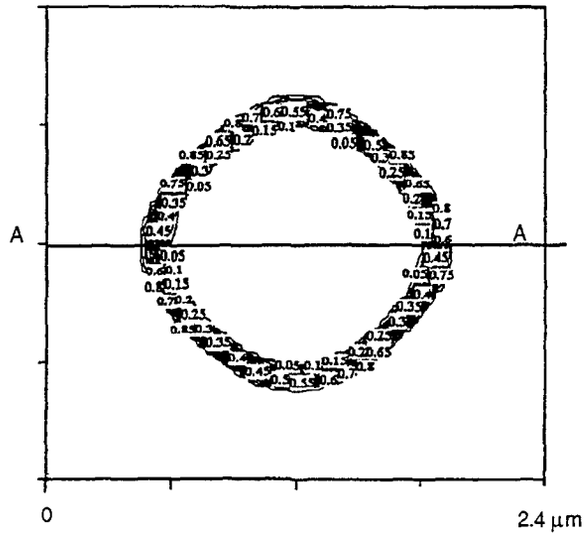

(b) Photoresist Thickness After Development

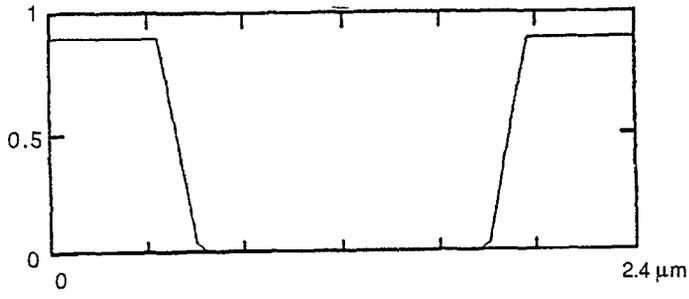

(c) Section A-A of the Remaining Photoresist

Figure 21
Photoresist values for N = 1 in Eq. (13).

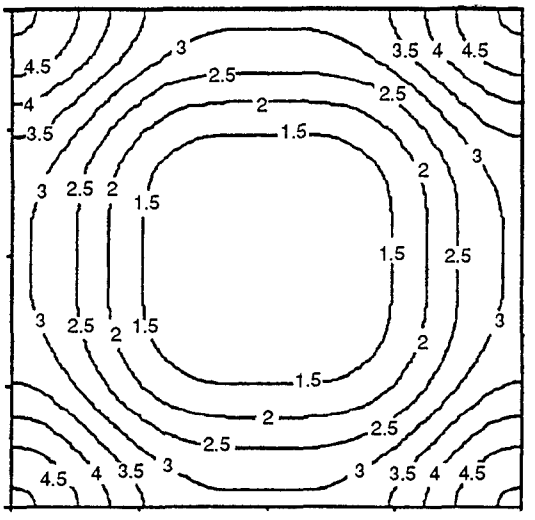

(a) 2-D Intensity Distribution

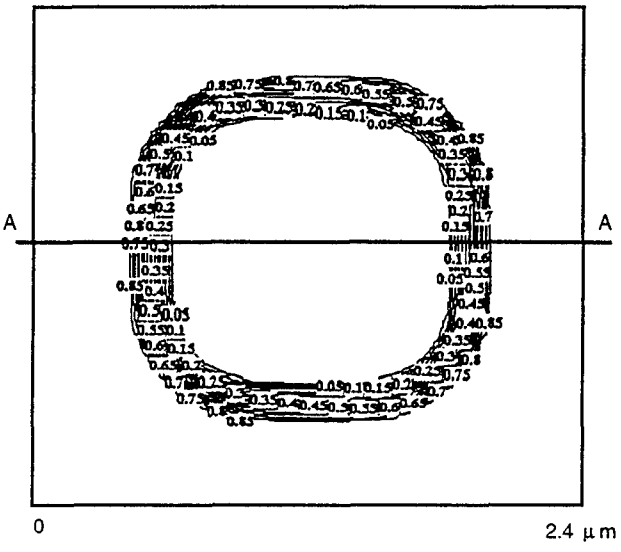

(b) Photoresist Thickness after Development

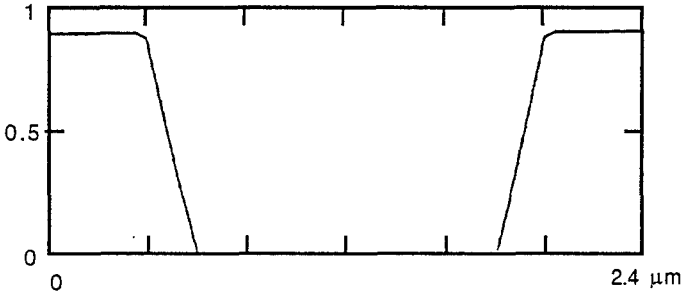

(c) Section A-A of the remaining photoresist

Figure 22
Photoresist values for N = 3 and M = 3.

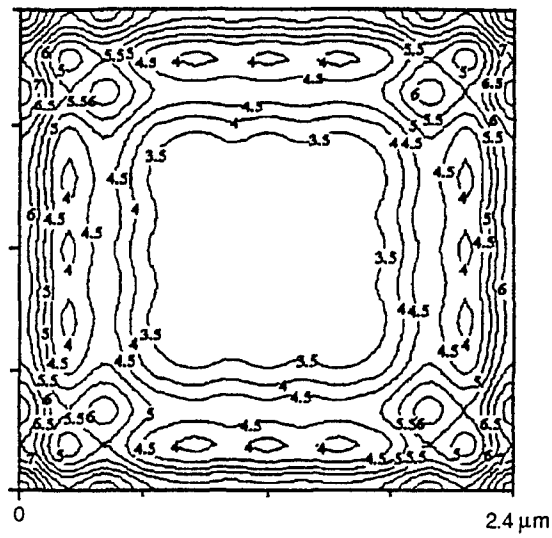

(a) 2-D Intensity Distribution

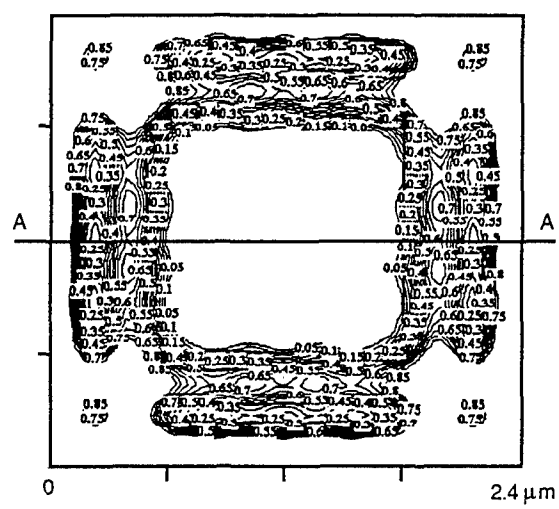

(b) Photoresist Thickness after Development

(c) Section A-A of Figure 23(b)

Figure 23
Photoresist values for M = 3, using the seventh harmonic.

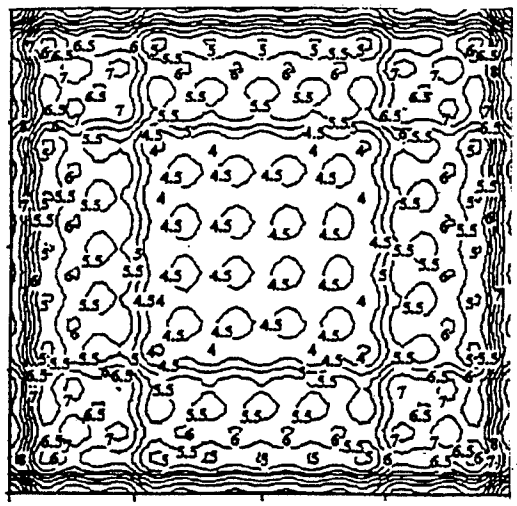

(a) 2-D Intensity Distribution

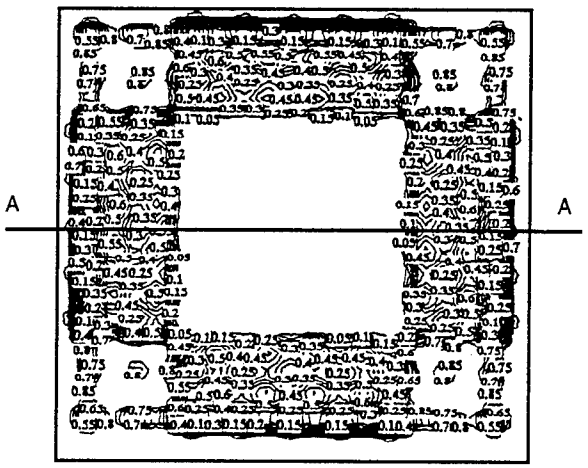

(b) Photoresist Thickness After Development

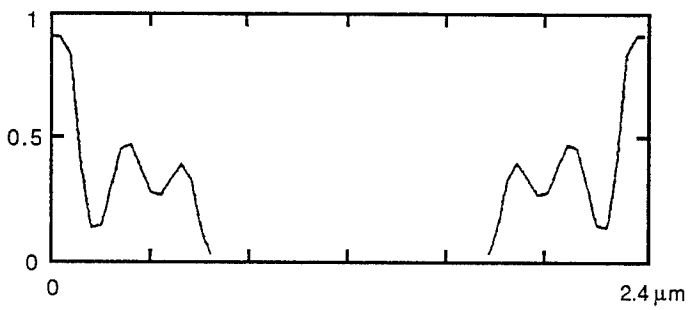

(c) Section A-A of Figure 24(b)

Figure 24
Photoresist values using ninth harmonic.

Using N = 9 and M = 7 improves D somewhat. For M = 7, D = 21% (see Figure 25).

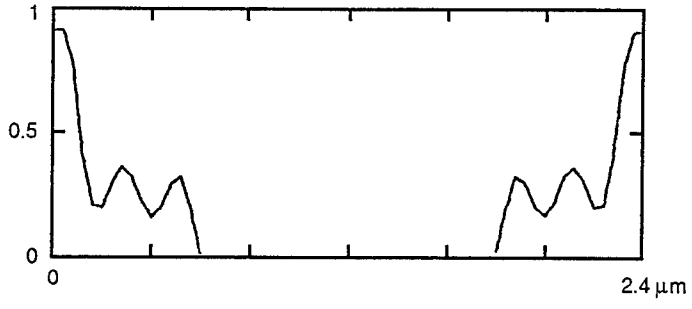

Figure 25
Section of image for N = 9 and M = 7.

It should be clear from this discussion that it is possible to choose the particular way of creating the image that best meets the requirements in a specific case.

10.0 INVESTIGATION OF HOW TO CREATE CROSS OBJECTS

This section of the report describes our efforts to create a periodic cross object, such as is shown in Figure 26, using the minimum number of harmonics.

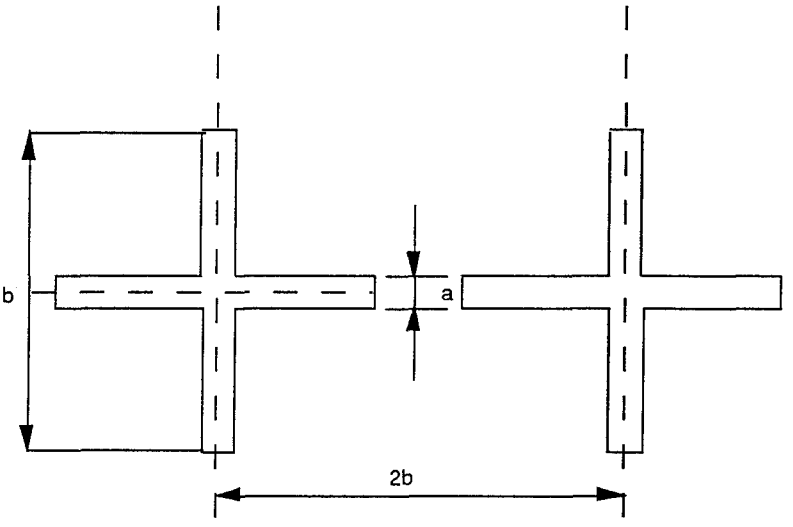

Figure 26
Cross object.

The Fourier spectrum of the cross object is defined by:

$$A(f_x,f_y) = ab \sin c(bf_x) \sin c(af_y) + ab \sin c(bf_y) \sin c(af_x) - a^2 \sin c(af_x) \sin c(af_y) . \quad (14)$$

The harmonics are calculated over a two-dimensional area with a step size of 1/2b.

For the case using harmonics with frequencies up to 5/2b for b = 5 μm and a = 1 μm, the image is shown in Figure 27. This image was created using harmonics without a positive constant bias equal to their amplitudes (i.e., mathematical, theoretical harmonics).

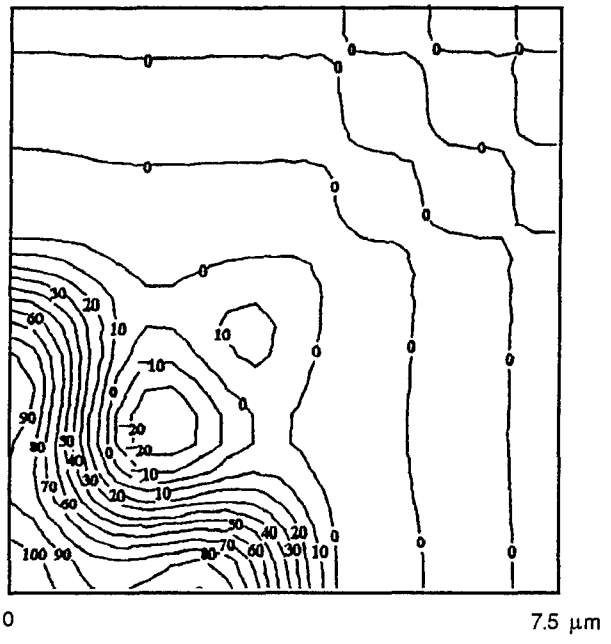

Figure 27
Intensity in the image of a cross object.

Figure 28 shows the result of creating a cross object using only the first 19 harmonics. All harmonics are positive, and it was not necessary to shift the mirror using this method. In the Fourier domain, the harmonics are as shown in Figure 29.

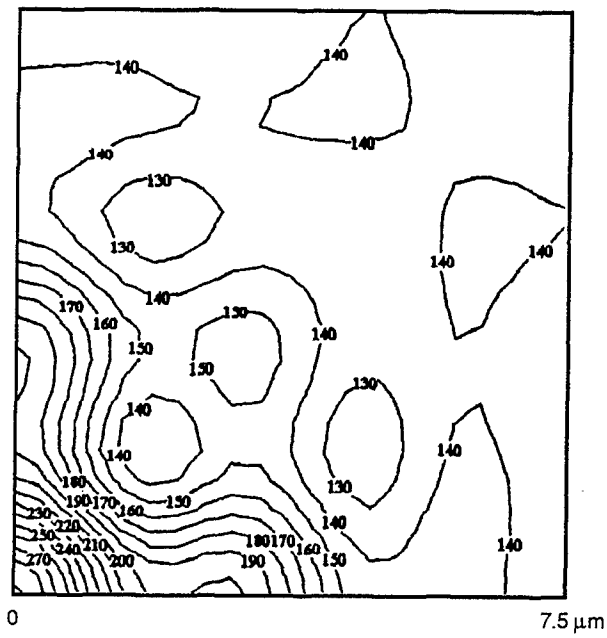

Figure 28
Intensity using a restricted number of harmonics.

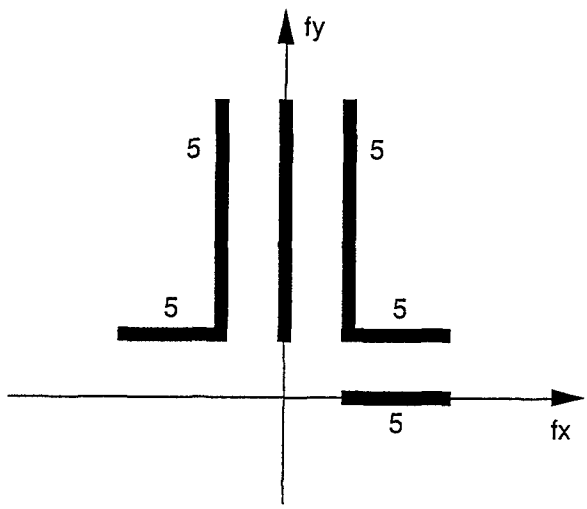

Figure 29
Locus of harmonics in Fourier domain.

The pattern shown in Figure 28 was created using only positive harmonics. Images generated using fewer harmonics did not yield satisfactory results. The large number of exposures required to generate cross objects points to the necessity of using a computer controlled setup.

11.0 FAILURE IN RECORDING IMAGES ON THICK FILM PHOTORESIST AND REASONS FOR THE FAILURE

In practice, the attempt to record a one-dimensional rectangular profile (see Figure 8) on thick film photoresist to produce the figure represented in Figure 9 produced the profile illustrated in Figure 31.

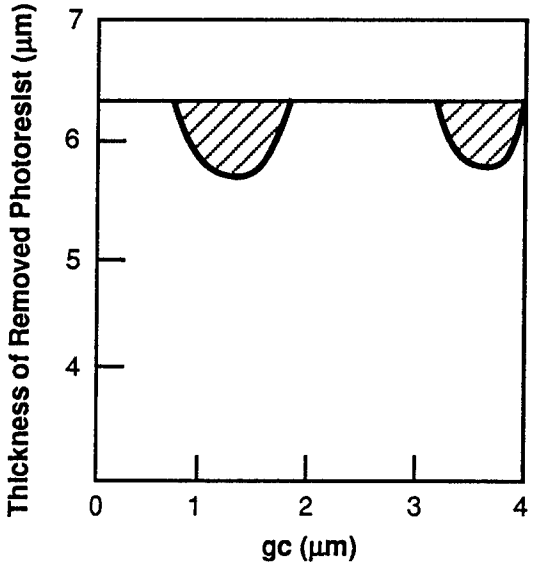

Figure 31
Actual form of the rectangular profile produced on photoresist.

In Figure 31 the diagonally hatched area represents the remaining photoresist. All material is removed down to a thickness of 6.3 μm. This result makes it clear that when using thick photoresist the depth response curve shown in Figure 6 is incorrect in the face of the complicated processes of exposure and developing.

In considering the real-world process of exposure, it is necessary to take into account that when light penetrates into the material of the photoresist the processes of absorption and exposure with respect to depth are distributed as a complicated function which depends on exposure on the surface of photoresist. The developing process proceeds as the propagation of a front, at every point having a speed of propagation which depends on exposure and which propagates in a direction normal to the wave front.

12.0 METHODS OF DETERMINING DEVELOPING SPEED

To determine the speed at which development propagates, it is useful to use the depth response data. The depth curve was determined by subjecting a thick film photoresist to calibrated doses of optical radiation through rectangular windows. After exposure, H_1, H_2, ..., H_n, the depth of removed material was measured (see Figure 32).

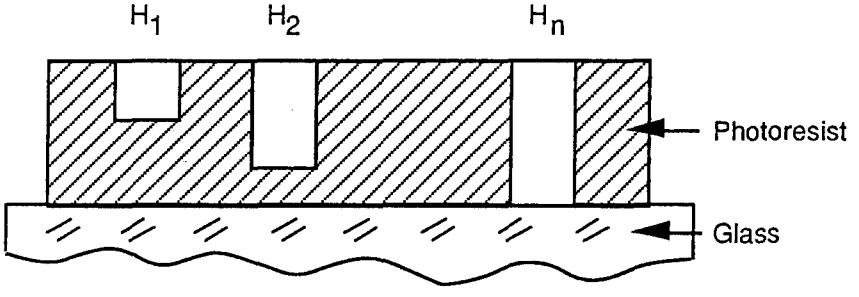

Figure 32
Measurement of thick film photoresist removed.

For this data to be useful, it is necessary to take into account the fact that photoresist has a considerable absorption coefficient at $\lambda = 0.404$ μm. The experiment demonstrated about 91% absorption through a path of 10 μm. If the propagation of the light in the absorption material is described in differential Eq. (15),

$$(dA)/A = -\mu \quad , \tag{15}$$

where A is the light incident on a thin layer of photoresist, then

$$\begin{aligned} d\ell_n(A) &= -\mu \quad , \\ \ell_n(A) &= -\mu s + c \quad , \end{aligned} \tag{16}$$

where s is the depth of the photoresist. It follows that

$$A(s) = e^{-\mu s + c} \quad . \tag{17}$$

In case of $S = 0$, $A(S) = A_0$, where A_0 is the exposure on the surface of the photoresist. Hence

$$A(s) = A_0 e^{-\mu s} \quad , \tag{18}$$

where μ is the coefficient of absorption. In our case, μ is about 0.24 if S is measured in μm. A comprehensive model of the exposure process would have to include changes induced in μ in the process of exposure, but our observation shows that μ changed insignificantly, so at this step of the investigation we can disregard that change.

Let us assume that in small ranges of exposure developing speed depends linearly on exposure. Let us divide the interval T of the developing time into N small intervals Δt_0. In this case we can represent the track S of developing process (depth of material removal) at time T_1 as

$$\begin{aligned} a_1 &= p_1 A_1 \Delta t_0 \\ a_2 &= p_1 (A_1 e^{-\mu a_1}) \Delta t_0 \\ a_3 &= p_1 (A_1 e^{-\mu(a_1 + a_2)} \Delta t_0) \\ s &= a_1 + a_2 + a_3 + \ldots \end{aligned} \tag{19}$$

The time interval T_1 in our experiment was the interval in which the developing processing reached a depth of H_1 (see Figure 32). As a first approach, let us assume $N = 1$. In this case, it follows from Eq. (19) that

$$p_1 = H_1/(A_1 T_1) \quad . \tag{20}$$

After we have a first approximation to p_1, let us insert p_1 in the exponent of Eq. (19) and calculate the new value of p_1:

$$p_1^{(i+1)} = H_1/\{A_1 \Delta t_0 + A_1 (e^{-\mu p_1^{(i)} \Delta t_0}) \Delta t_0 + \ldots \} \quad , \tag{21}$$

where i is the iteration cycle. This method soon brings $\Delta p = | p_1^{(i+1)} - p_1^{(i)} |$ close to zero. When we begin to consider the next exposure A_2 on the surface of a photoresist (see Figure 32) with a depth of development H_2, let us assume that we know the developing speed between point K and point L (see Figure 33), where point K is the point at which exposure A_2 will be attenuated with respect to the absorption process to a value of A_1 (see Figure 33).

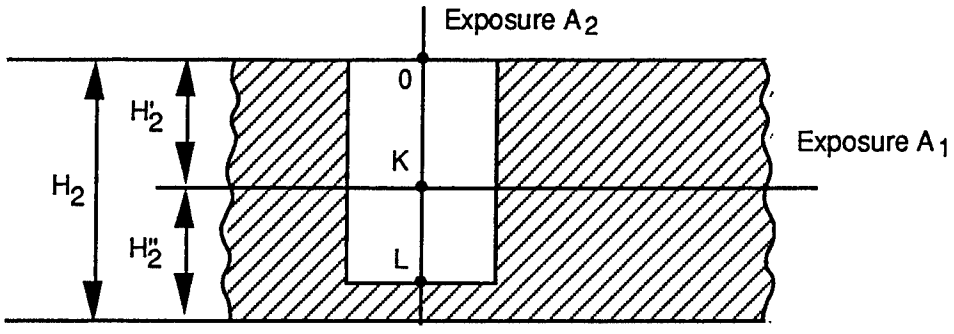

Figure 33
Process of developing given an exposure A_2 on the surface.

If we know the developing speed in area KL (see Figure 33), we can determine the time required for the developing process in that area. Let us take a small interval of time Δt_0 (in our software we used $\Delta t_0 = 0.005$ sec) and consider the process of developing from point K to point L as the sum of the tracks of the process of developing.

$$S_N = \sum_{i=1}^{N} p_1 A_1 e^{-\mu S_{i-1}} \Delta t_0 \quad , \qquad (22)$$

$$S_0 = 0$$

When S begins to exceed H_2'' (see Figure 33) the process must be stopped. This defines the time $KL = N\Delta t_0$. Now that we know the developing time for developing from 0 to K, we can iterate the process described above to determine the constant p_2, the characteristic developing speed for exposure A_2. By applying this method to all the results of measuring the depth curve, we can obtain the curve of the developing speed as a lump linear function. The result of this process after smoothing this function using spline interpolation is presented in Section 13.

13.0 THE PROPAGATION OF THE DEVELOPING FRONT

The propagation of the developing front is a complicated, nonlinear process. All the available computer simulation power is necessary for understanding the processes which take place in the photoresist and for defining the conditions for obtaining high quality images.

In order to simulate the propagation of the developing front, it was necessary to develop special purpose software. The propagation of the developing process was considered step by step,

addressing unequal time intervals based on the precision of the expected results. Considering the one-dimensional process, assume that we have an exposure function f(x) on the surface of the photoresist (see Figure 34).

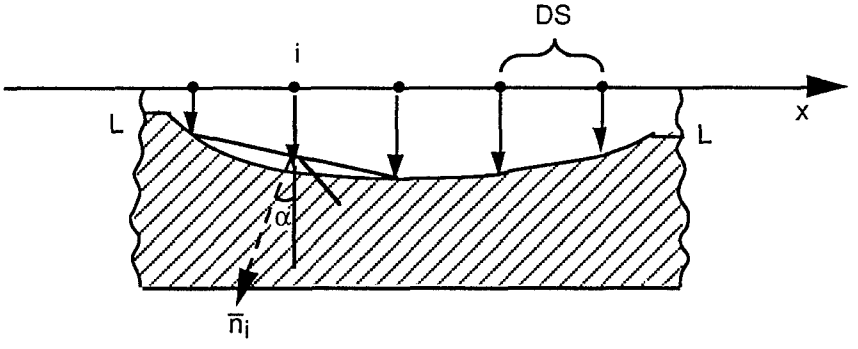

Figure 34
First step of developing front propagation.

At every point i on the photoresist surface, the front of the developing process will propagate a distance ΔS_i.

$$\Delta S_i^0 = v_i \Delta t_0 \quad , \tag{23}$$

where v_i is the propagation speed of developing, which depends on the exposure function f(x). After this first step it is necessary to determine the effective exposure on the line of the developing front LL (see Figure 34) using the value of ΔS_i and Eq. (16), in which the value of A is f(x). The direction $\bar{n}_i$ of front propagation at every point i is determined using the points i-1 and i+1 in Figure 34.

$$\tan(\alpha) = [\Delta S_{i+1} - \Delta S_{i-1}]/(2DS) \quad , \tag{24}$$

where DS is the step between each two points on the original surface of the photoresist. If we know the effective exposure at point i and the direction of propagation of the developing process, we can infer the location of the next step of front propagation

$$\Delta S_i^1 = v_i^1 \Delta t_1$$
$$x_i^1 = (i-1)DS - \sin\alpha \Delta S_i^1$$
$$S_i^1 = S_i + \cos\alpha \Delta S_i^1 \quad , \tag{25}$$

where Δt_i is the time interval determined at the point at which we have maximum exposure and given an interval Δt_i of propagation of the developing process, $\Delta S_{max} < 0.01$ μm. After applying Eq. (25), we join the points which we have obtained with the spline function to derive the value of S_i at points x_i = (i-1)DS, and repeat the calculations.

Based on this theoretical approach, we developed software to model the propagation process. Figure 35 presents the exposure curve, which is significant in the area of the cutoff level -- this is necessary to minimize errors in the size of the final image. The most significant areas are 0.5 μm < × < 0.7 μm and 1.7 μm < × < 1.9 μm.

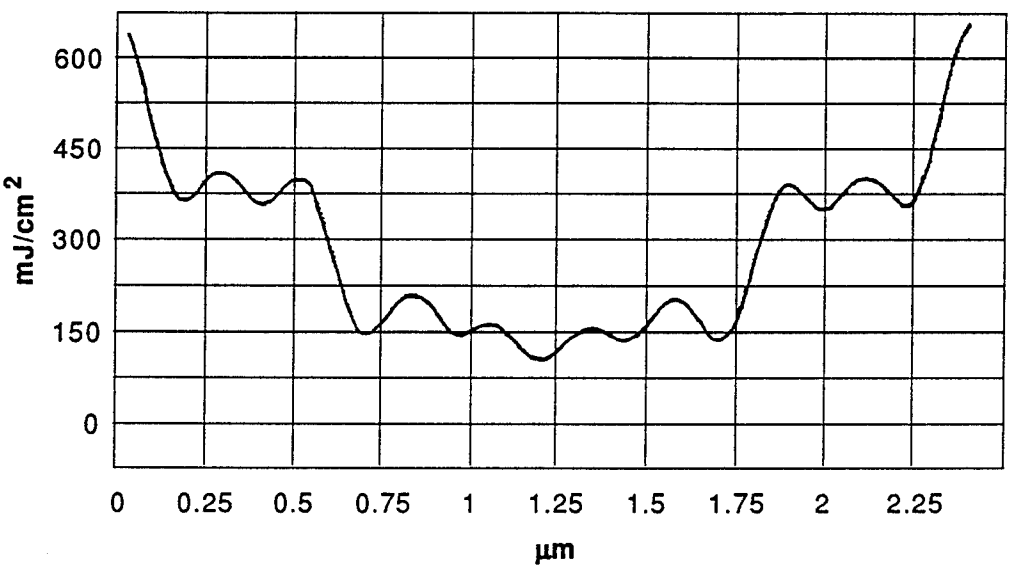

Figure 35
Exposure curve.

Figure 36 plots the speed of developing.

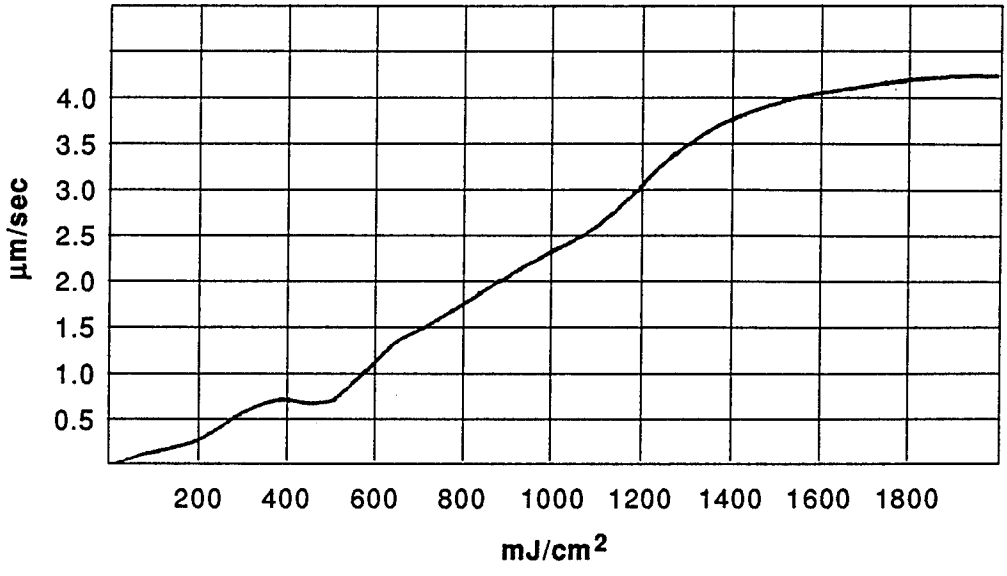

Figure 36
Developing speed.

Computer analysis showed the first steps of propagation corresponding with the exposure curves. Figures 37 and 38 show the developing process at 0.12 sec and 0.2 sec.

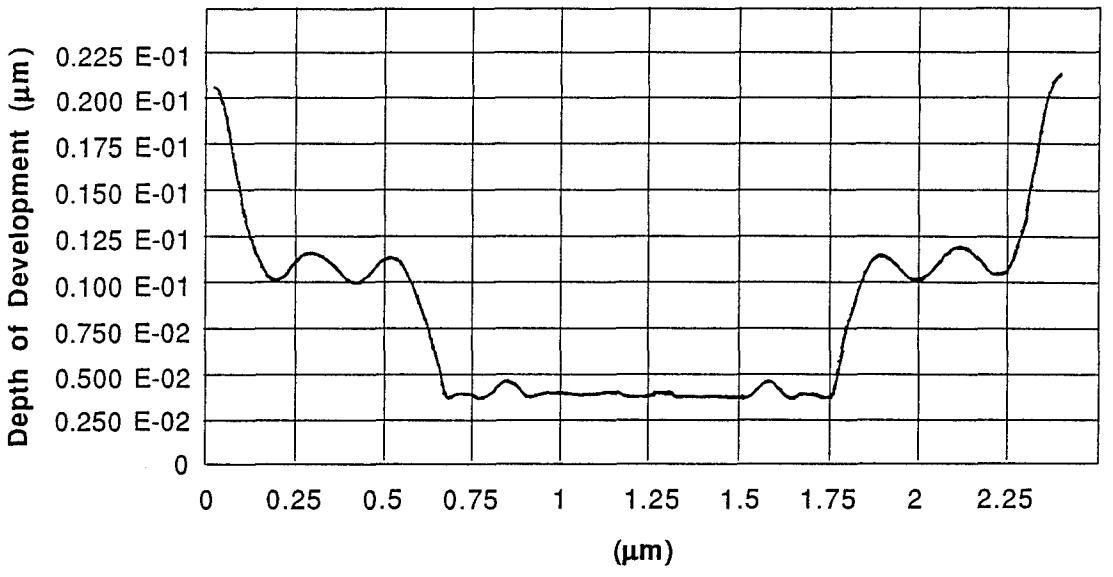

Figure 37
Depth of development (time = 0.12 sec).

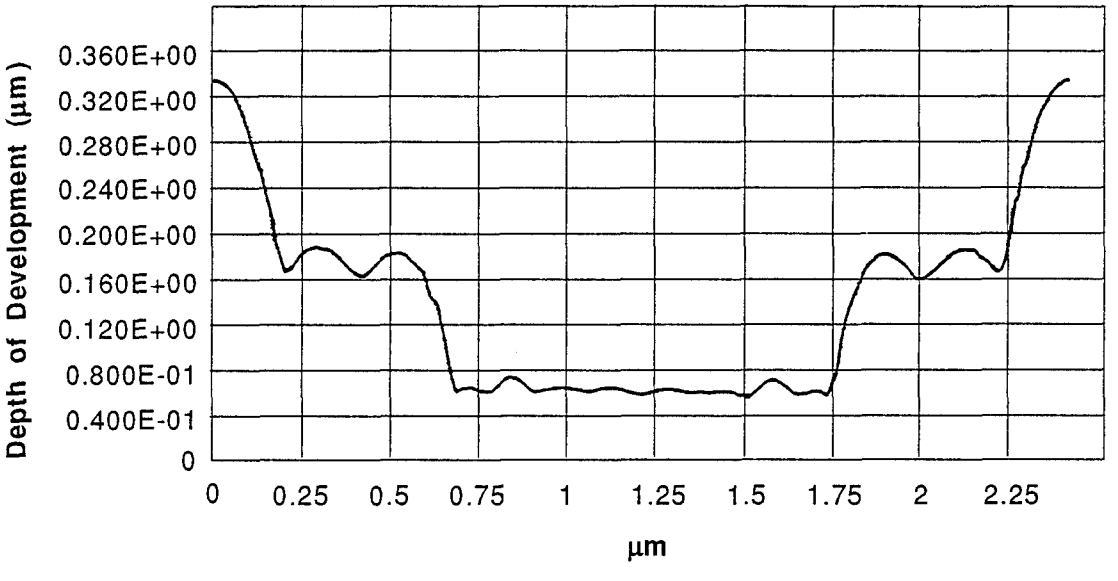

Figure 38
Depth of development (time = 0.2 sec).

Later, the form of the front propagation begins to lose its original characteristics as shown in Figures 39 and 40.

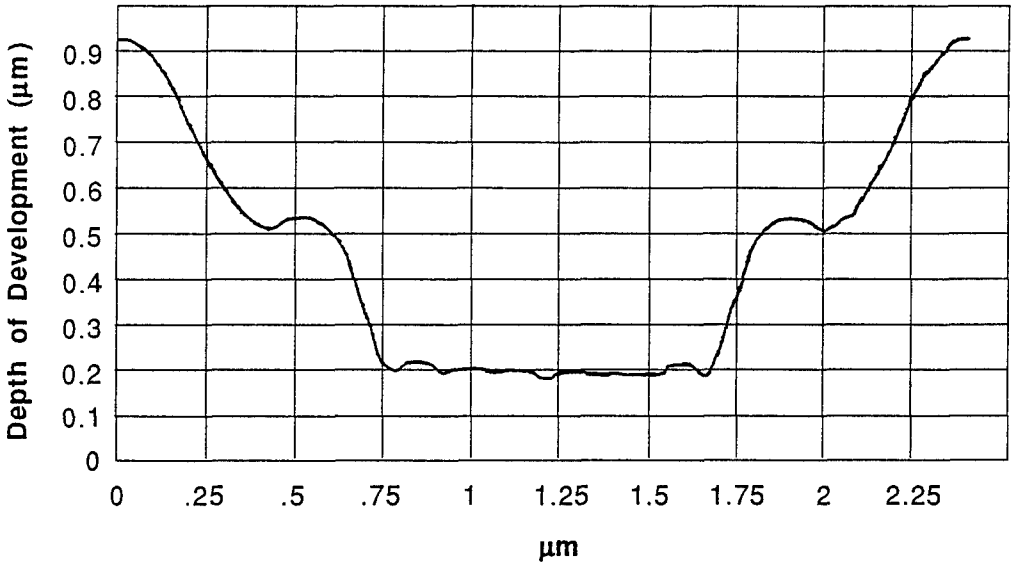

Figure 39
Depth of development (time = 0.616 sec).

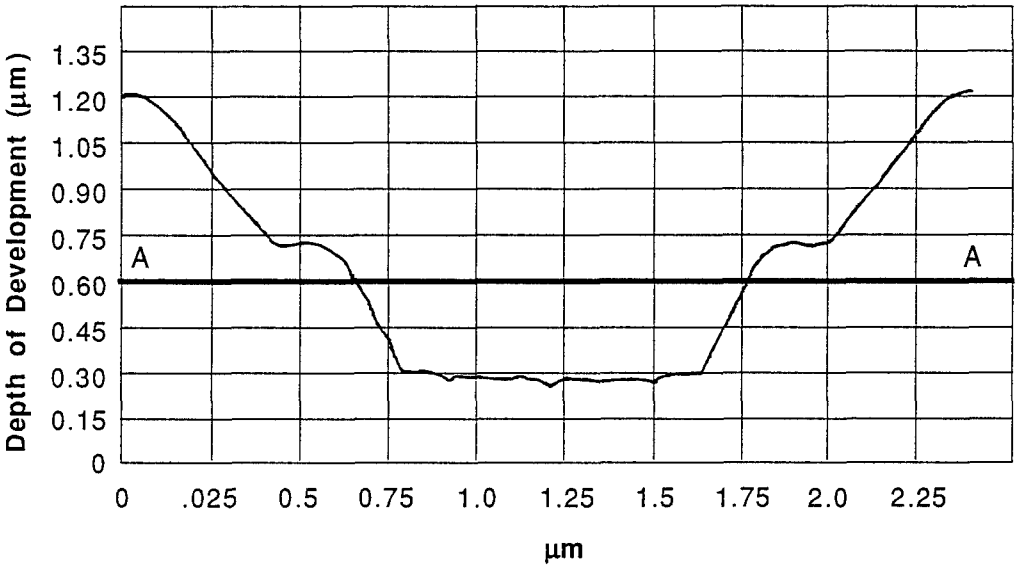

Figure 40
Depth of development (time = 0.84 sec).

The form in Figure 40 we can reasonably consider as the limiting case in front propagation when we have a sufficient value of deviations of the cutoff level AA. The thickness of the film is 0.6 μm (line A-A in Figure 40). After this moment, the form of the propagation front degenerates quickly, as shown in Figures 41 and 42.

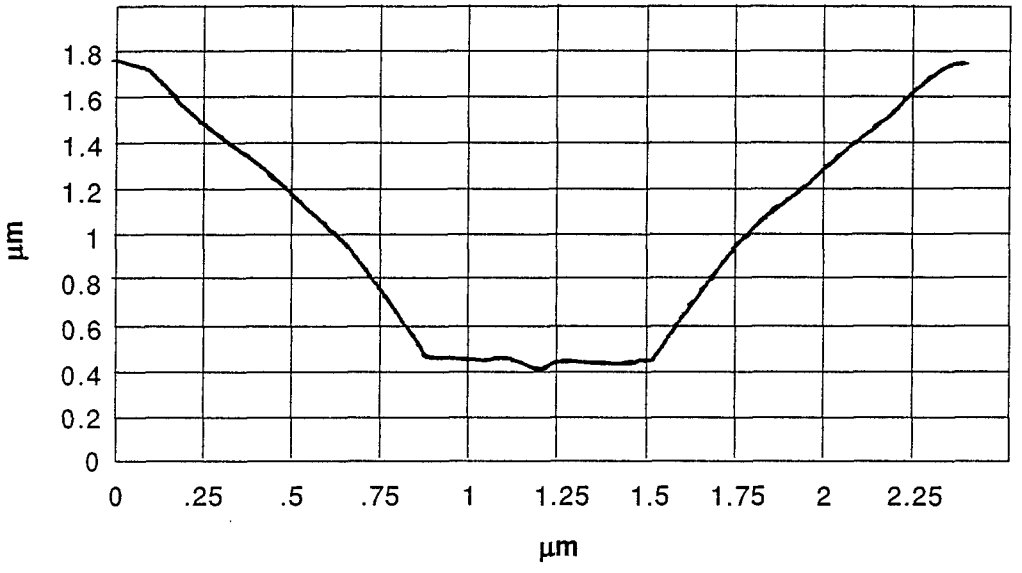

Figure 41
Depth of development (time = 1.32 sec).

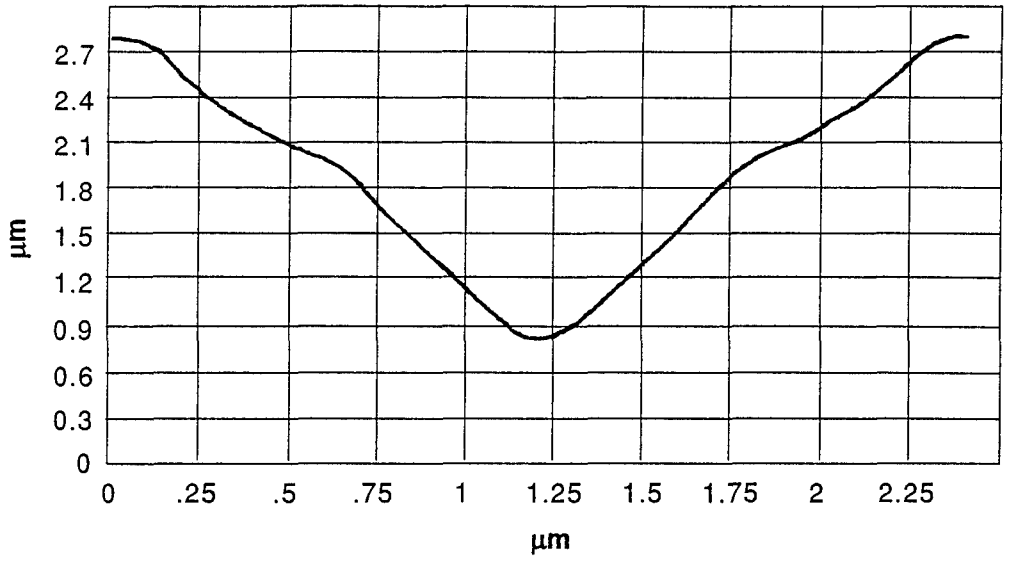

Figure 42
Depth of development (time = 2.7 sec).

The results in Figure 42 explain the failure described in Section 11 of this report. To produce an image with acceptable quality we cannot use photoresist with a thickness of more than 0.6 µm.

14.0 HARDWARE

This project clarified the most appropriate design for a setup for creating images of ~20 mm using a collimator and a translated source of radiation so as to create interfering flat beams. This design is shown in Figure 43.

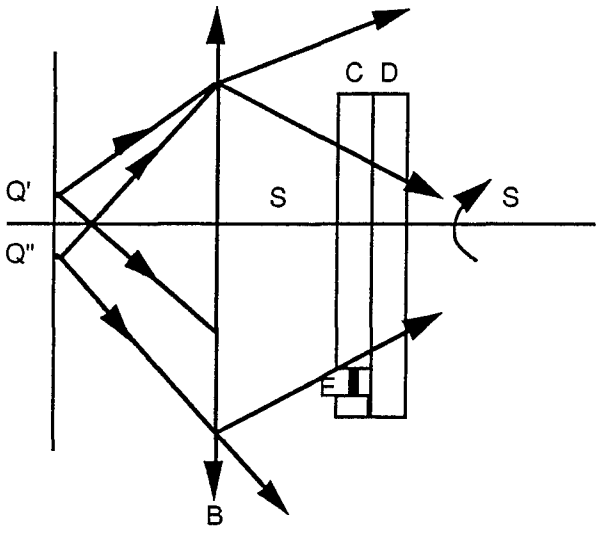

Figure 43
Setup with collimator for small images.

In Figure 43, B is the collimator lens, D the photoresist, C the frame holding the photoresist, and E the piezoelectric translator to produce negative harmonics. The table can be rotated to create a two-dimensional image. The Line SS is the axis of rotation.

The variable shift of the sources is introduced by the acousto-optic filters L' and L" in Figure 44, which illustrates the setup for controlling the beams.

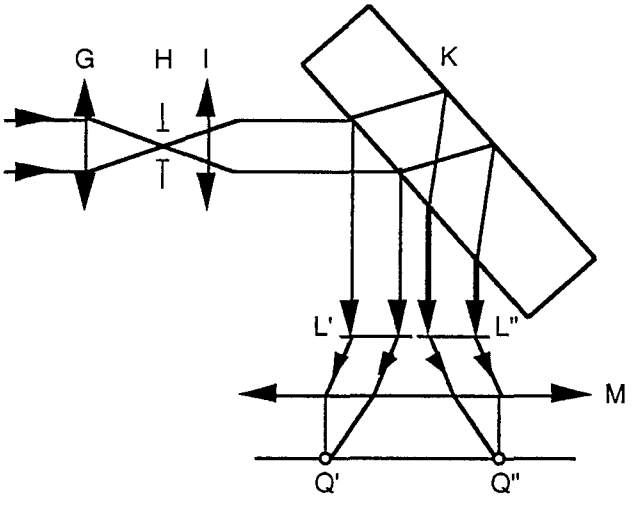

Figure 44
Design to guide work beams.

The collimated laser beam, after spatial filtering at H, strikes the flat plate of glass, (K) which functions as a beam splitter. L' and L" are acousto-optic deflectors with variable frequency. M is the objective of the auxiliary system. Q' and Q" are the sources in the focal plane of collimator B (see Figure 43).

We were unable to create a large collimator with a field of view of about 80°. We were only able to produce a collimator about 50 mm in diameter. To use beams about 100 mm to 200 mm in diameter we propose the setup shown in Figure 45.

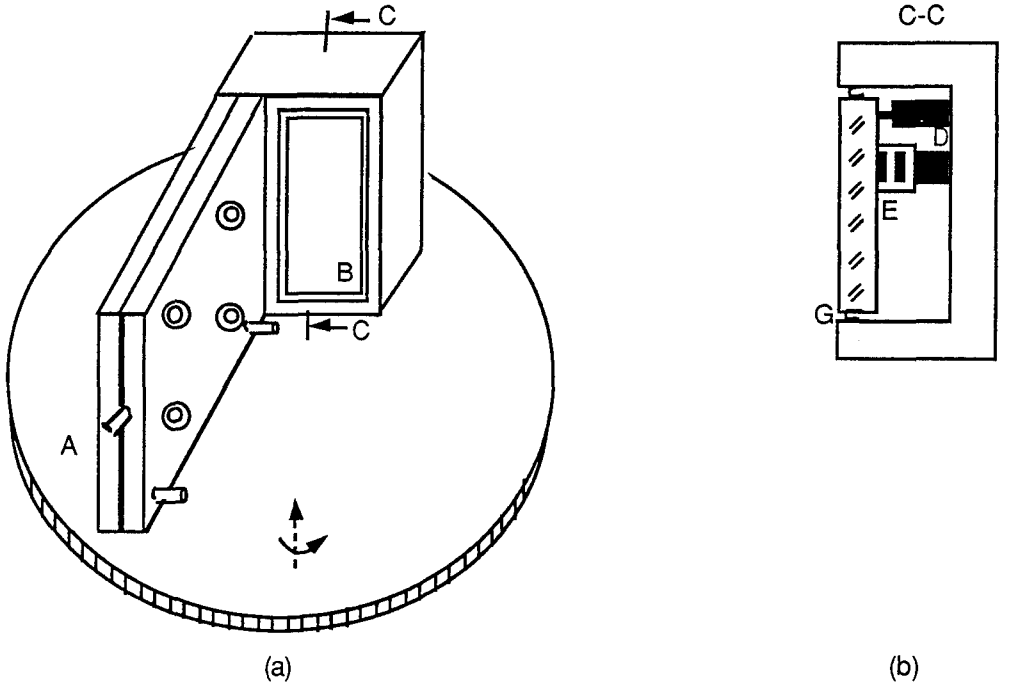

Figure 45
Setup with flat mirror.

The photoresist-covered plate is held in place using a vacuum device, the exit of which is shown as A in Figure 45. The mirror B is attached to the body via the flexible membrane G. Mirror translation and precision positioning is performed by using the piezoelectric translator D and capacitive sensor E.

A wide array of problems are avoided by confining ourselves to a device with beams not more than 300 mm in diameter. These problems involve deformations of the flat mirror in the shifting

process. The design will require detailed study of how to assemble a large flat mirror. Assembly would be more complicated than shown in Figure 45(b), and would include means to alleviate the vertical load on the mirror.

15.0 RECORDING SETUP

The recording setup is shown in Figure 46.

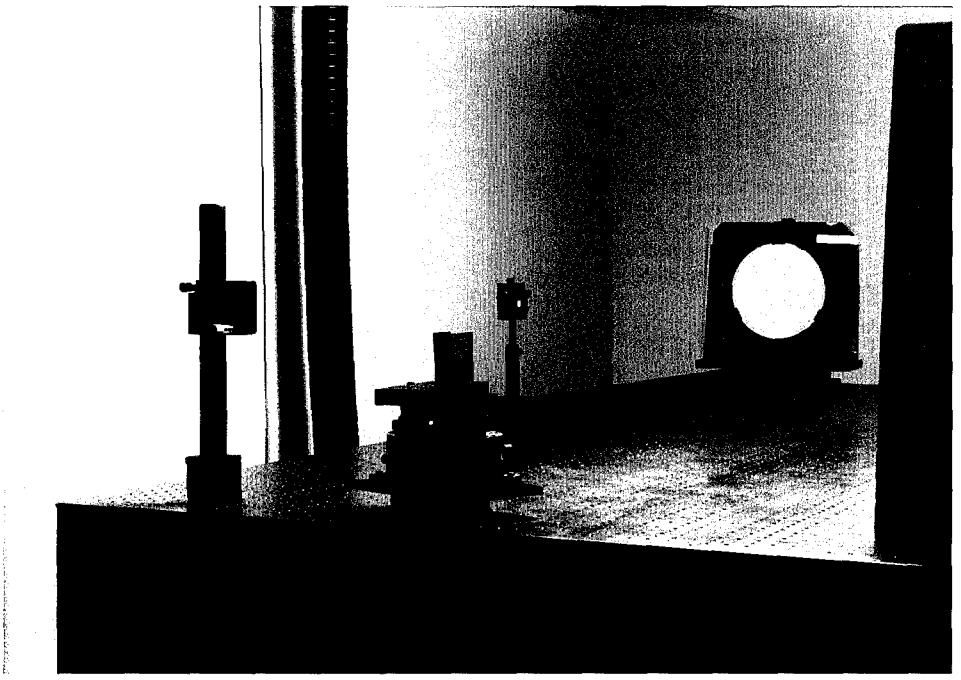

Figure 46
Recording setup.

The laser beam is expanded using a Newport 4X objective with a 15 μm pinhole. The expanded beam is then collimated using a 10-inch off-axis mirror. The recording plate is illuminated by the collimated beam (see Figure 47).

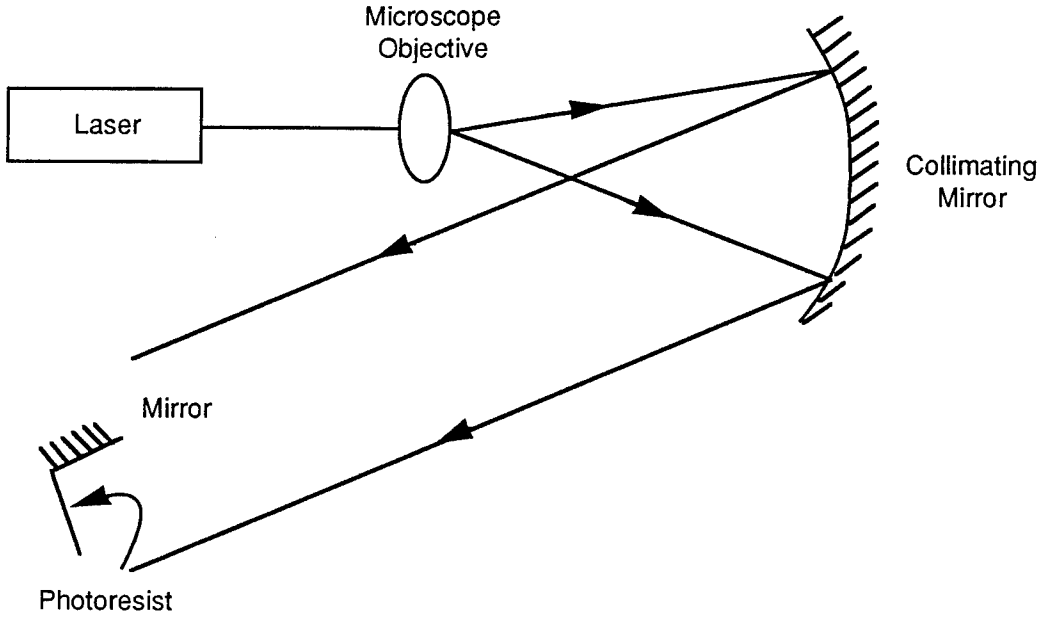

Figure 47
Schematic of recording setup.

A total of nine exposures were made on each sample. The angles and exposure energies used are shown in Table 4.

Table 4 Exposure Energies at the Nine Angles

Angle	Exp. Energy (mJ)
4° 56'	42.35
9° 55'	5.28
14° 59'	0
20° 10'	5.28
25° 32'	12.65
31° 09'	5.28
37° 08'	0
43° 37'	5.28
50° 55'	9.35

After exposure, each plate was developed using the following method. The spray development cycle for 0.6 μm coating of Shipley 1400-30 resist is as follows:

Develop:	8s
Overlap:	2 s
Rinse:	15 s
Dry:	15 s

Plates were baked at 115°C for 30 minutes and then examined under a microscope. One plate is shown in Figure 48.

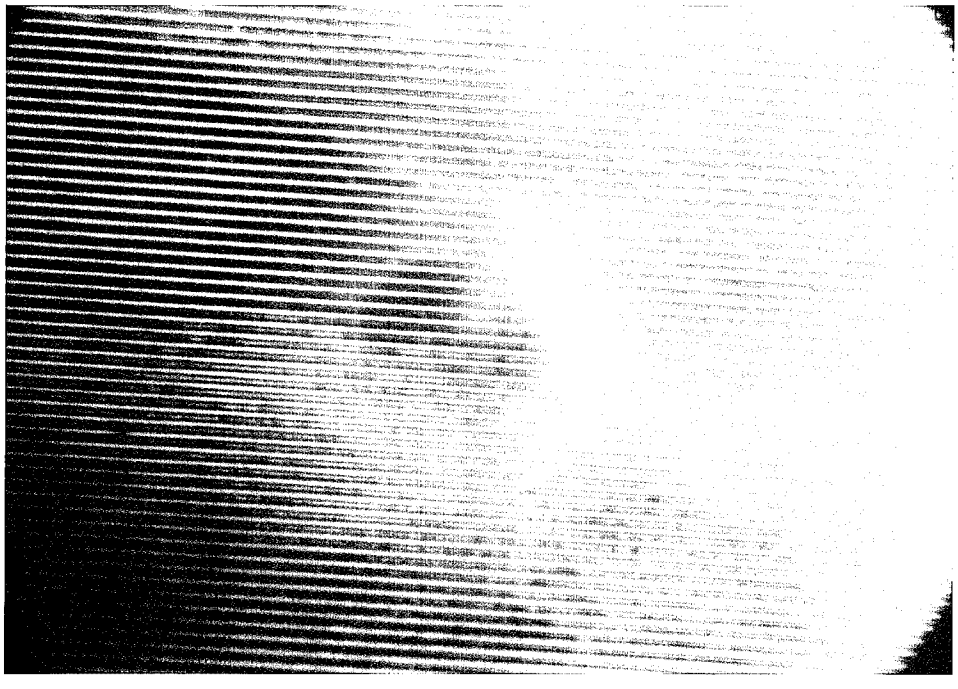

Figure 48
Photograph of recorded pattern (magnification 1000X).

Figure 48 clearly shows the high-quality pattern structure. The bright stripes are photoresist, the grey ones glass. The dark narrow stripes surrounding the photoresist are the slope of our ridges. The sharp angle of the slope shows dark, the refraction angle exceeding or close to the aperture of the microscope.

Our next step was to examine the samples using a scanning electron microscope. The photographs in Figure 49 were taken using a JEOL Model 6100 scanning electron microscope. The magnification is 10,000X, and the sample is tilted 70° from normal. The scale is 1 cm = 1 μm. In the top photograph, the photoresist has been scraped in one section to get a better view of the profile of our pattern. As seen in the bottom photograph, the grating period is 2.4 μm with a 50% duty cycle. Also, the shape of the photoresist stripes is trapezoidal as expected from our calculations (Figure 40). At this point we are unable to measure the slope of the edges; we will need to have an outside company perform these measurements.

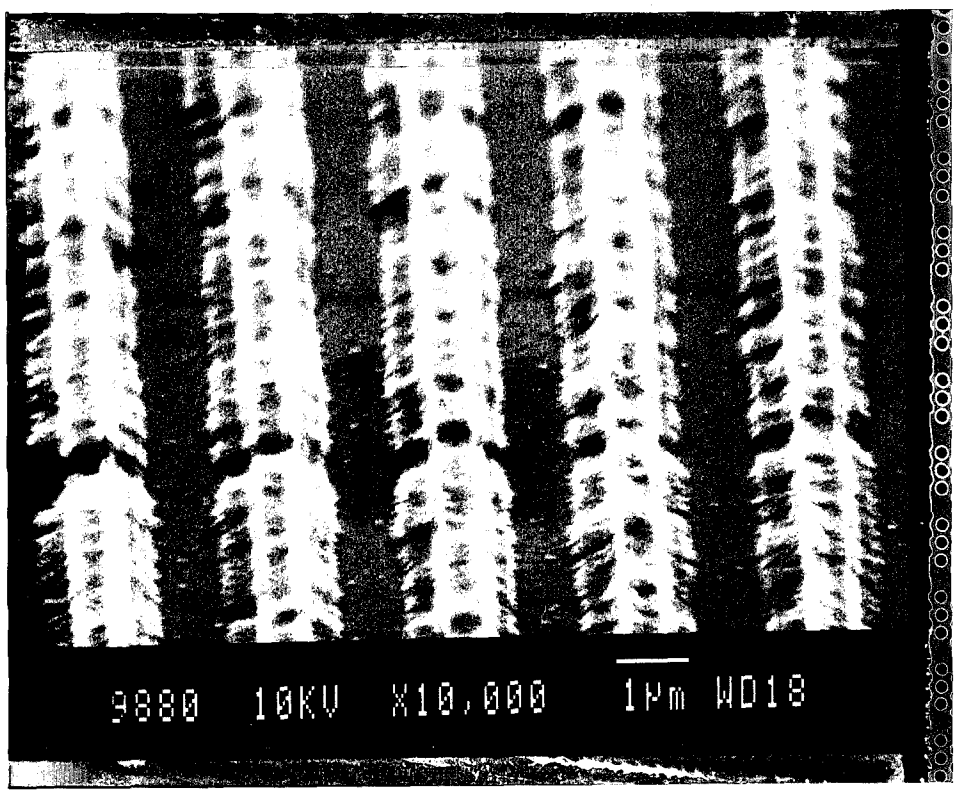

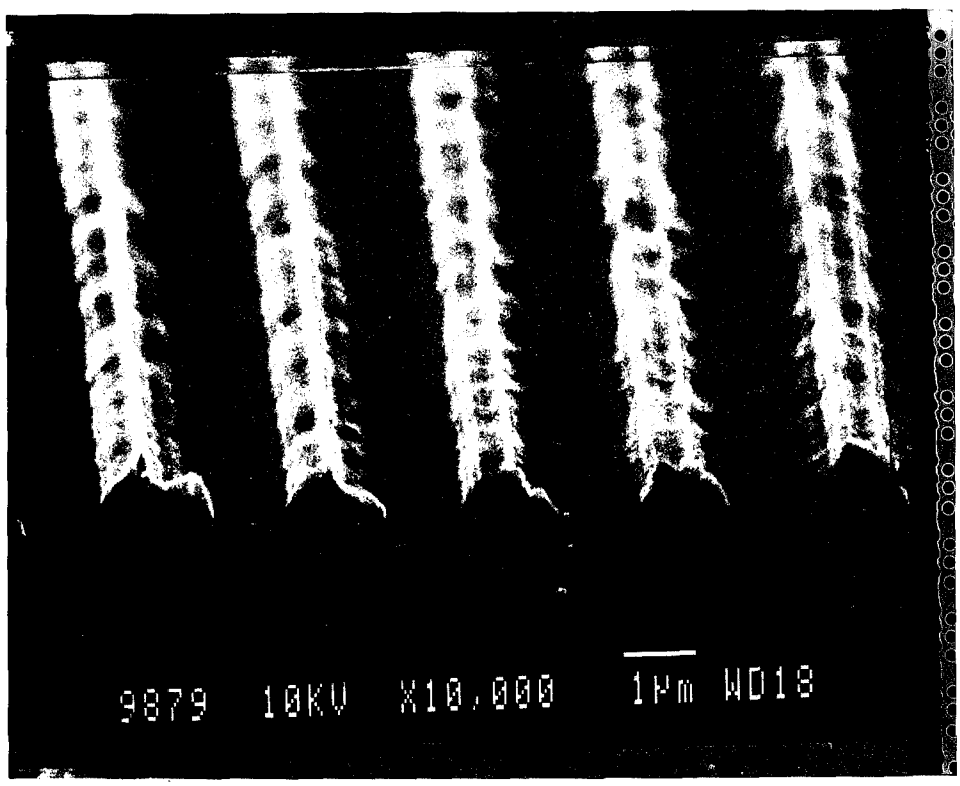

Figure 49
Photographs taken from JEOL 6100 SEM magnification 10,000X.

16.0 CONCLUSIONS

(i) POC has developed a methodology for creating high contrast images with low sensitivity to variations in exposure and developing time, using a small number of exposures. The results encourage us to believe that we can create industrial devices for the production of flat panel displays without using traditional projection lithographic technology with all its inherent drawbacks.

(ii) A comprehensive computer model of photoresist multiple exposure has been developed and experimentally confirmed.

(iii) Experimental demonstration has confirmed our simulation of the lateral propagation of the photoresist development process.

(iv) We completely designed and experimentally validated the proposed technologies.

The preliminary investigations have defined the issues which are to be taken up in the next stage of this project.

16.1 Theoretical Issues

1. Further investigation is needed into the process of exposing and developing photoresist material. Detailed investigation will consider the influence of the coefficient of absorption on exposure.

2. Investigation is needed into the minimum number of harmonics necessary to create a complex two-dimensional image.

3. We will investigate the possibility of creating an image on a photoresist device in the presence of back surface reflection.

16.2 Design Issues

1. Design a wide field-of-view collimator lens for an acousto-optics device .

2. Investigate the possibility of introducing a second axis of rotation of the mirror assembly in the flat-mirror setup to create complex two dimensional images.

3. Investigate the possibility of designing a large setup with interference beams larger than 500 mm.

17.0 REFERENCES

1. S. H. Zaidi and S. R. Brueck, "Multiple-Exposure Interferometric Lithography," J. Vae. Sci. Tech., vol. 11, no. 3, pp. 658-674 (1993).

2. D. H. Zigen, C. A. Mack, and R. Distasio, "Generalized Characteristic Model for Lithography: Application to Negative Chemically Amplified Resists," Opt. Eng., vol. 31, no. 1, pp. 98-104 (1992).

Supplemental Literature

1. A. B. Cohen and P. Walker, "Polymer Imaging," in Imaging Processes and Materials," edited by J. M. Stuge, N. Y. VNR, pp. 226-261 (1989).

2. G. Beresin, A. Nikitin, R. Suris, "Principles of Optics Lithography," in Radio and Communication, Moscow (1982).